Regulation of excitation#contraction coupling at the Drosophila neuromuscular junction

Published in final edited form as:

J Physiol. 2022 January ; 600(2): 349–372. doi:10.1113/JP282092.

Regulation of excitation-contraction coupling at the *Drosophila* neuromuscular junction

Kiel G. Ormerod[1,†], **Anthony E. Scibelli**[2], **J. Troy Littleton**[1]

[1]The Picower Institute for Learning and Memory, Department of Biology, Department of Brain and Cognitive Sciences, Massachusetts Institute of Technology, Cambridge, MA

[2]Department of Biology, Tufts University, Medford, MA.

Abstract

The *Drosophila* neuromuscular system is widely used to characterize synaptic development and function. However, little is known about how specific synaptic alterations effect neuromuscular transduction and muscle contractility that ultimately dictate behavioural output. Here we develop and use a force transducer system to characterize excitation-contraction coupling at *Drosophila* larval neuromuscular junctions (NMJs), examining how specific neuronal and muscle manipulations disrupt muscle contractility. Muscle contraction force increased with motoneuron stimulation frequency and duration, showing considerable plasticity between 5–40 Hz and saturating above 50 Hz. Endogenous recordings of fictive contractions revealed average motoneuron burst frequencies of 20–30 Hz, consistent with the system operating within this plastic range of contractility. Temperature was also a key factor in muscle contractility, as force was enhanced at lower temperatures and dramatically reduced with increasing temperatures. Pharmacological and genetic manipulations of critical components of Ca^{2+} regulation in both pre- and post-synaptic compartments impacted the strength and time-course of muscle contractions. A screen for modulators of muscle contractility led to identification and characterization of the molecular and cellular pathway by which the FMRFa peptide, TPAEDFMRFa, increases muscle performance. These findings indicate *Drosophila* NMJs provide a robust system to correlate synaptic dysfunction, regulation, and modulation, to alterations in excitation-contraction coupling.

Keywords

Drosophila ; synapse; neuromuscular junction

Introduction

Neuromuscular systems that regulate stereotyped motor behaviours are composed of multiple component parts that interact in a highly coordinated and synchronized fashion to control muscle contraction and displacement (Selverston, 1980; Goulding, 2009). Central

Correspondence and requests for materials should be addressed to K.G.O. (kormerod@mtsu.edu).
†Current address: Department of Biology, Middle Tennessee State University, Murfreesboro, TN.

Footnote: publication; bioRxiv: doi: https://doi.org/10.1101/2020.07.09.196261

The authors declare no competing interests.

pattern generators (CPGs) initiate stereotyped behaviours such as locomotion, feeding, and swimming (Katz and Frost, 1995; Schwarz *et al.,* 2017). CPGs relay rhythmic output through interneurons to motoneurons, controlling the timing and magnitude of muscle contraction (Selverston, 2010). In turn, the peripheral nervous system (PNS) signals the dynamic state of the muscle back to the CPG to modulate circuit output (Singhania and Grueber, 2014). A large body of work on the composition and regulation of these components comes from invertebrate studies in crayfish, leech, locust, crab, and lamprey (Marder *et al.,* 2005; Marder and Bucher, 2007; Nusbaum, Blitz and Marder, 2017). *Drosophila melanogaster* has become a popular genetic system to dissect and explore the composition and regulation of many of these components, including CPGs (Song *et al.,* 2007; Clark *et al.,* 2018), interneurons (Hasegawa, Truman and Nose, 2016), and sensory neurons (Song *et al.,* 2007; Singhania and Grueber, 2014). Despite these efforts, studies directly examining the role of excitation-contraction coupling (ECC) in locomotion are limited in *Drosophila* (Lehmann and Dickinson, 1997; Paterson, Anikin and Krans, 2010; Ormerod *et al.,* 2013; Milakovic *et al.,* 2014; Ormerod, Krans and Mercier, 2015; Ormerod, Jung and Mercier, 2018; Aponte-Santiago *et al.,* 2020; Sun *et al.,* 2020), though many of these components have been examined in other insects and arthropods (Atwood, 1967; Usherwood, 1967; Hoyle, 1983; Worden, 1998; Belanger, 2005).

Locomotion is one of the most well studied rhythmic behaviors, including in *Drosophila* (Caldwell *et al.,* 2003; Saraswati *et al.,* 2004; Hughes and Thomas, 2007; Song *et al.,* 2007; Cheng *et al.,* 2010; Clark *et al.,* 2018). *Drosophila* larval locomotion encompasses different types of movements (e.g. turning, rolling, burrowing), though motivated linear crawling is the most highly stereotyped and orchestrated repetitive patterned behaviour produced from identical contraction waves (Hughes and Thomas, 2007; Heckscher, Lockery and Doe, 2012). Muscles directly below the cuticle contract, then relax, to propagate peristaltic contraction waves from the posterior to the anterior of the larvae. These peristaltic waves are achieved by systematic, coordinated contractions of bodywall muscles, predominately those in abdominal segments (Clark et al, 2018). *Drosophila* larvae are bilaterally symmetrical with stereotyped abdominal hemisegments composed of 30 individual muscle fibers. Each muscle is a viscerally-located, supercontractile (contracting to a length less than 50% of resting length) striated multinucleated muscle fiber (Keshishian *et al.,* 1996b) attached directly to the cuticle through apodemes (Koh, Gramates and Budnik, 2000). Canonical muscle fiber contractility is controlled via postsynaptic glutamate receptors activated by glutamate released by synaptic vesicles (SVs) from presynaptic motoneuron terminals (Harris and Littleton, 2015). Approximately 36 motoneurons per hemisegment innervate the abdominal musculature. Three different motoneuron subtypes are present: type I, which releases glutamate from SVs; type II, which predominantly contain large dense core vesicles (DCVs); and type III, which innervate muscle 12 and release insulin-like peptides (Budnik, 1996; Hoang and Chiba, 2001). The neuromuscular junction (NMJ) is a critical site of plasticity and can be regulated by neuromodulators released directly from motoneuron terminals or centrally into the open circulatory system as hormones (Ormerod *et al.*, 2013; Milakovic *et al.,* 2014; K. G. Ormerod, Jung and Mercier, 2018). Type I motoneurons are rhythmically active during waves of muscle contractions underlying forward and reverse locomotion (Newman *et al.,* 2017). Motoneuron activity is dictated by the neuronal input

received from descending interneurons, whose firing pattern is ultimately controlled by the locomotor CPGs within the ventral nerve cord (VNC) (Fox, Soll and Wu, 2006; Zarin *et al.,* 2019).

To further dissect ECC and its link to locomotion, we employed a force transducer with 10 μN resolution and a unique motoneuron-stimulation paradigm to characterize the dynamic output of the neuromuscular system and how plasticity in synaptic function manifests in changes to muscle output. Synaptically-driven muscle force increases with stimulation frequency and duration, with elevation of either component leading to increased force. However, continued increase in either factor ultimately causes saturation in muscle force. The most robust plasticity in muscle contractility occurs between 5 and 40 Hz stimulation. Fictive contraction recordings from larvae with the CNS intact revealed endogenous contraction kinetics were between 20–30 Hz, where the greatest plasticity exists. Subsequently, critical roles for Ca^{2+} regulation in contractility were examined by genetically and pharmacologically altering Ca^{2+} channel function pre-and postsynaptically, as well as Ca^{2+} liberation from internal stores. Temperature was also found to have a critical effect on muscle contraction. A screen for muscle force modulators revealed the neuropeptide, TPAEDFMRFa, increases muscle performance. The effects of the neuropeptide on muscle contractility and pathway components though which it operates were characterized. These data directly relate synaptic function with ECC, providing insights into how key NMJ proteins contribute to muscle contractility.

Materials and methods

Drosophila stocks

Drosophila melanogaster were cultured on standard medium at 21°C at constant humidity in a 12:12 light:dark cycle. Wandering 3rd instar larvae of both sexes were used for experimentation. The following lines were used (Bloomington *Drosophila* Stock Center, BDSC; Vienna *Drosophila* Research Center, VDRC): Canton S. was used for all control experiments, elav-GAL4 (BDSC 458), *mef2-GAL4* (BDSC 27390), ryanodine receptor (BDSC 65885), cac-RNAi (VDRC, 104168), FMRFa receptor RNAi (VDRC v9594), Dromyosuppressin receptor 1 RNAi (VDRC v9369), Dromyosuppressin receptor 2 RNAi (VDRC v49952).

Dissection

Wandering 3rd instar larvae were isolated from the sides of culture vials and dissected in modified hemolymph-like (HL3) saline. Two *Drosophila* salines were examined (Feng et al., 2004). The first Hemolymph-Like saline HL3 has the following composition (in mM): NaCl: 70; KCl: 5; CaCl2:1.5; MgCh: 20; NaHCOs: 10; Trehalose: 5; Sucrose: 115; HEPES: 5, (pH = 7.18). The second saline, HL3.1, has the same composition but [$MgCl_2$] was reduced to 4 mM. Larvae were pinned dorsal side up at the anterior and posterior ends, a small incision was made along the entire dorsal midline and the visceral organs were removed. All nerves emerging from the central nervous system (CNS) were severed at the ventral nerve cord, and the CNS and ventral nerve cord were removed. In some experiments, the orientation of the larvae prior to initial dissection was altered depending on which muscles were examined.

To examine the dorsal muscles, the animal was pinned ventral side up and dissected along the ventral midline. To examine the lateral muscles, the animal was pinned lateral side up (muscle fiber 4 at the apex) and dissected along the lateral most point.

Electrophysiology

Excitatory junctional potentials (EJPs) were elicited by stimulating severed abdominal nerves. A Master 8 A.M.P.I. (Jerusalem, Israel) stimulator was used to elicit stimulation via a suction electrode (A-M systems, Sequim, WA). EJPs were recorded using sharp glass microelectrodes containing a 2:1 mixture of 3M potassium chloride:3 M potassium acetate, with an electrode resistance of 40–80 MQ. An Axoclamp 2B amplifier (Molecular Devices, San Jose, CA) was used for signal detection and digitized via Axon Instruments digidata 1550 (Molecular Devices). Signals were acquired at 10 kHz using Clampex and processed using Clampfit and MiniAnalysis.

Nerve-evoked contraction force recordings

All force recordings were obtained using the Aurora Scientific 403A force transducer system (Aurora Scientific, Aurora, Canada), including the force transducer headstage, an amplifier, and digitizer. Nerve-evoked contractions were generated using bursts of electrical stimuli from a Master 8 (A.M.P.I.) stimulator. The duration of single impulses was 5×10^{-4} s and the interburst duration was kept constant at 15 s. Burst duration and frequency were altered for each individual experiment. Using a suction electrode, severed motoneuron branches innervating abdominal segments were stimulated. Each preparation was visually inspected to ensure a minimum of 5 abdominal segments were contracting. Larvae were dissected as outlined above. To attach larvae to the force transducer, a hook was made from a fine minuten pin and placed onto the posterior end of the larvae. Digitized data was acquired using Aurora Scientific software, Dynamic Muscle Acquisition Software (DMCv5.5). The digitized data was imported and processed in Matlab using custom code written by A. Scibelli. Temperature was controlled using a CL-200A heater-cooler controller (Warner Instruments, Hamden CT) with a heat sink (Koolance) that regulates temperature via feedback from a thermocouple placed directly next to the animal to enable control within 0.1 °C. Temperature was rapidly modified by constant perfusion of physiological saline though a Harvard apparatus in-line saline temperature controller (Holliston, MA) and a Warner Instruments dish temperature regulator (Model TB3 CCD).

Pharmacological agents

Felodipine (Sigma, F9677), ryanodine (R&D systems, 688286), thapsigargin (Thermofisher, T7458), and caffeine (Sigma, C0705) were applied directly to exposed larval preparations by bath application during force recordings.

Statistical analysis

Statistical analyses were performed using GraphPad Prism (San Diego, CA, USA). Graphing was done using Matlab, Microsoft Excel, or GraphPad Prism. Statistical significance was determined using specific statistical tests as indicated in the text. Asterisks denote p-values

of: *, p< 0.05; **, p< 0.01; and ***, p< 0.001, except where otherwise noted in the text. All histograms and measurements are shown as mean ± SD except where noted in the text.

Data availability

The data in this manuscript are available from the corresponding author upon reasonable request.

Results:

Force-recordings

To explore the contractile properties of *Drosophila* 3rd instar larval NMJs, muscle contractions were elicited in semi-intact preparations with the CNS removed. A force transducer with 10 μN resolution was modified to attach to the posterior end of a larvae (Figure 1A). Previous studies in *Drosophila* examined contractile properties by continually stimulating motoneurons at the same intraburst frequency and duration (Ormerod *et al.,* 2016). An example of a single contraction induced from the setup, highlighting the amplitude, rise tau, and decay tau is shown in Figure 1B. To systematically characterize muscle contraction performance, bodywall contractions were induced by stimulating motoneurons at a frequency within the physiological range of 40 Hz for 600 ms duration every 15 s (0.067 Hz) for up to one hour. Muscle responses were robust with steady-state contractions recorded after 1 hour of stimulation showing only a 29.2 ± 9.6% reduction in force over this period (Figure 1C). Endogenous muscle contractions are driven by neuronal input whose firing pattern is ultimately controlled by locomotor CPGs within the ventral nerve cord (VNC) (Song *et al.,* 2007). We recorded fictive locomotor patterns from bodywall muscles via intracellular recordings from semi-intact preparations with the CNS and VNC left intact (Figure 1D). These patterned outputs displayed wide intraburst frequency variability from 1 to 150 Hz. Given the variable output of endogenous activity, we explored a more dynamic approach to eliciting muscle contractions to determine the range of force bodywall muscles were capable of producing under a variety of motoneuron stimulation frequencies.

Stimulation frequency impact on contractions

Initially, 25 impulses were delivered to motoneurons and the stimulation frequency was varied from 1 to 150 Hz. For each experiment, 6 replicate contractions were induced at each stimulation frequency, followed by the next stimulation frequency, et cetera (Figure 1E). Contractions were averaged across the 6 replicate stimuli for a given stimulation frequency and the resulting trace with 95% confidence interval (CI) was determined (Figure 1F). Twenty-five stimuli at 1 Hz stimulation induced 3.5 ± 1.1% of the maximum force produced at 150 Hz, while 2 Hz stimulation was sufficient to induce 5.2 ± 1.1% of the maximum force. Force generation at 2 Hz was not greater than 1 Hz stimulation. In contrast, 25 stimuli at 5 Hz produced a resultant force of 11.0 ± 1.1% of the force at 150 Hz, indicating this stimulation frequency is sufficient for temporal summation for enhancing contractile force. From 10 to 50 Hz, a nearly linear increase in force was produced at each successive increase in stimulation frequency (10, 15, 20, 25, 30, 40, 50 Hz), producing a maximal force at 50 Hz. Increasing stimulation frequency beyond 50 Hz resulted in a reduction in force

production. Therefore, when total stimuli number remains constant, increasing stimulation frequency increases force production until saturation is reached at 50 Hz.

Effect of stimulus duration and frequency on contractions

Although 50 Hz drove maximal muscle contraction, it was unclear whether the saturation of force generation was a consequence of stimulus frequency or stimulus duration. To explore this relationship further, burst duration was held constant at 600 ms and the frequency of stimulation was varied from 1 to 150 Hz. Figure 1G depicts the raw data from each individual contraction within a single trial, and Figure 1H depicts averaged traces from the replicate stimuli at a given stimulation frequency with a corresponding 95% CI. Force-frequency curves were then generated from this stimulation paradigm and plotted as a percentage of the magnitude of force generated at the highest stimulation frequency of 150 Hz (Figure 1I). Under these conditions, 5 Hz stimulation produced a force of 6.0 ± 3.1% of that produced during 150 Hz stimulation (Table 1). Comparable to prior experiments, force production increased in a linear fashion as the frequency increased from 10–50 Hz. However, increasing stimulation frequency to 100 and 150 Hz also enhanced the force. Thus, both the duration and frequency of stimulation are critical factors in determining the absolute magnitude of force production.

To further explore the relationship between stimulus frequency and stimulus duration, we generated a series of force-frequency curves by keeping the burst duration constant through an entire experiment over 200, 250, 300, 500, 600, 750, 900, 1000, 2000, or 5000 ms while increasing stimulation frequency from 1 to 150 Hz. Each of the independent force-frequency curves for a given burst duration generated a sigmoidal curve similar to what was observed at 600 ms (Figure 2A and Table 1). The overall pattern from stimulation force recordings revealed that increasing stimulus frequency or duration results in a progressive and gradual increase in muscle force production. In all experiments, a single action potential was sufficient to induce a contraction that was between 2.6 and 3.3% of the 150 Hz contraction force (note that 1 Hz stimulation at 1000, 2000, and 5000 ms corresponded to 2, 4, and 10 stimuli respectively). Given force saturates at or above 100 Hz for all stimulus durations, there should be no difference between these conditions once force reaches maximal. Thus, it is not surprising that the greatest difference between stimulus durations are seen from 10 to 50 Hz, where considerable plasticity in muscle performance occurs (Fig 2A). Plotting the percent difference between stimulation durations as a function of stimulus frequency generated a bell-shaped curve with peak differences observed at 25 Hz. The greatest effect of stimulus duration was observed at 25 Hz, where an increase from 200 to 5000 ms resulted in a 70.3% increase in muscle force. Figure 2B depicts an overlay of 25 Hz stimulation from 200, 300, 600, 900, and 2000 ms. A critical feature of the dataset is reflected in the stimulation frequency required to generate half-maximal force (50%) for each stimulus duration, where a linear decrease in the stimulus frequency required to reach 50% is observed (Table 1). Plotting the 50% max value as a function of stimulus duration generated a strong negative correlation (R^2=0.9) with a slope of −0.016, indicating every 100 ms increase in duration shifts this value to the left by 1.6 Hz. Despite the dramatic effects that stimulation duration has on force production below 50 Hz, the saturated or maximum raw force generated from a 200 ms duration stimulus was not significant for any

of the longer stimulus durations (Figure 2C, D, one-way ANOVA, P=0.654, N=6–7). These findings indicate maximal force from *Drosophila* bodywall muscles can be generated by a 200 ms stimulus delivered at 100 Hz.

Stimulation duration and frequency effects on contraction kinetics

To examine the effects of stimulus duration and frequency on the time-kinetics of contractions, data from four representative stimulation durations were explored: 200, 300, 600, and 900 ms (Figure 2E-G). Rise tau kinetics revealed no significant difference at 100 and 150 Hz (Figure 2E, one-way ANOVA, 200 vs 900, P=0.13, N=3). Significant differences between groups were observed between 10 and 50 Hz, which correlates well with force plasticity (Fig 2E, one-way ANOVA, P<0.0001, F=19.12, N=3). Rise tau kinetics decreased below 15 Hz in the 600 and 900 ms duration groups due to spatial summation dynamics reaching rise tau during the few stimuli. Figure 2F shows the time-to-peak data for the four representative stimulus durations. Time-to-peak data revealed similar results to the rise-tau data for the 200 and 300 ms duration groups, while a frequency vs. time-to-peak analysis revealed no correlation (R^2-values of 0.32 and 0.06, respectively). The time-to-peak data also showed no correlation with frequency (R^2-value 0.01). The 900 ms duration data revealed that above 40 Hz stimulation, contractions reached peak force prior to the end of the stimulus train. The time-to-peak values for the four groups, averaged across all stimulus frequencies was 302, 447, 674, and 923 ms respectively. Excluding the 900 ms data set, where a time-to-peak value was achieved prior to the end of stimulation, an average of 75–150 ms of muscle contraction was observed following termination of the stimulus. Given rise tau represents the time to reach ~63% of the maximal value, a linear rise in contractile force would predict a 37% increase in time from tau-rise to time-to-peak. The difference between these two parameters was calculated and averaged for each representative group across all stimulation frequencies, generating differences of 57, 63, 82, and 110%. These data indicate greater force saturation occurs during longer duration stimulus trains. Plotting the decay tau data revealed few differences across stimulation durations (Figure 2G), with an average decay tau value of approximate 200 ms.

Size and orientation effects on contractile force

Throughout the experiments, some variability was noted in the total raw force generated from one preparation to the next (Fig 2C), differing in magnitude by up to 50%. Given this variability, one potential contributor to the differences in force generation was larval size. To examine this variable, the length and width of 91 larvae was measured and the total force generated by each animal was determined by eliciting a 100 Hz stimulus for 600 ms (Figure 3A-B). Larval contraction force was then plotted against length, width, area, and volume to determine if these physical parameters correlated with overall force production. None of these metrics revealed a positive correlation with contractile force (Figure 3C, D), indicating larval size does not have a significant effect on the total force generated from 3rd instar larval preparations (two-tailed Pearson's correlation; width: r=0.01462, P=0.8906; length: r=−0.1246, P=0.2391, N=91).

We next explored whether recruitment of different muscle fibers altered muscle performance or maximal force generation (Figure 3E-H). To examine contribution from distinct muscle

groups, larvae were dissected in three different orientations: i) along the dorsal midline where ventral muscle fibers 6, 7, 12, and 13 contribute predominately to longitudinal force production; ii) along the ventral midline where dorsal fibers 1, 2, 3, and 4 contribute principally; or iii) a lateral incision where lateral fibers 3, 4, 12, and 13 contribute primarily (Figure 3E, F). All three larval orientations displayed nearly identical force-frequency curves (Figure 3G), indicating performance was not significantly different across distinct muscle groups (one-way ANOVA, P= 0.18, N=8–9). In addition, maximum force generated from muscle contraction elicited by stimulation in each larval orientation was similar (Figure 3H, one-way ANOVA, N=8, P=0.17).

Fictive recordings reveal endogenous contractile properties

Force recordings from larvae with their CNS left intact were conducted to examine endogenous contraction properties (Figure 4). Figure 4A depicts a sample fictive force recording. Data from seven animals were compiled and the average burst duration, interburst duration, and magnitude of force was determined (Figure 4B-D). Endogenous contractions were typically multi-component, with varying durations generated by asynchronous contractions from different abdominal hemisegments. Burst durations were calculated from the onset of a contraction to the return to baseline. The resulting values ranged from less than 1 s to 25 s, with an average of 10.4 s (Figure 4B). Small contractions (<1 mN) likely reflect few or single, asynchronous contractions of individual abdominal segments. Quantifying interburst duration demonstrated most fictive contractions are immediately followed by another contraction (<1 s between contractions, 132/223 contractions). Binning of interburst durations for contractions >1 s into 5 s windows revealed a greater propensity for shorter duration contractions compared to long (Fig 4C). Quantifying the magnitude of force recordings demonstrated a wide range of force values from 0.2 mN to 7.4 mN, with an average of 2.8 mN (Figure 4D). A correlation between contraction duration and force was not observed, as evident from an R^2 value of 0.037. To dissect the endogenous stimulation frequency driving the excitation-contraction machinery, contractions that were single-component (example trace, Figure 4E) were binned into time-to-peak windows reflecting the 600 and 900 ms duration data sets from Fig 2 E-F (600: 600–700; 900: 840–1000 ms). Given the observed duration of endogenous contractions, short (200 and 300 ms time-to-peak) duration contractions were rare and not included in the calculations. The rise tau was calculated from each contraction and extrapolated onto the curves from Figure 2E to estimate endogenous stimulation frequency (Figure 4F). The average rise tau for the 600 and 900 ms bins was 407 and 506 ms respectively, correlating to endogenous stimulation frequencies of 27.2 and 22.4 Hz (Figure 4F, inset). Taken together, the endogenous contraction machinery generates robust and frequent contractions. On average, contractions reach roughly half of the maximal force value attainable (Figure 2), while the endogenous stimulation frequency is approximately half of that required to generate maximal force. Thus, the endogenous contractions machinery operates robustly, though a substantial capacity for modulation of force production still exists.

Temperature effects on contraction dynamics

To examine the effect of temperature on muscle performance in control larvae, contractions were generated using 600 ms duration bursts at 40 Hz every 15 seconds and plotted as

a percentage of force generated at room temperature (22°C). Surprisingly, decreasing the temperature from 22°C to 16°C increased contraction force, with a peak increase of 29.4 + 4.9% observed at 17°C (Figure 5A). Increasing temperature from 22°C to 39°C gradually decreased the force of contraction until a complete failure at 40 Hz was observed at and above 32°C in some preparations. Representative traces from a single trial showing the effects of temperature on muscle contraction are shown in Figure 5B. Calculating the Q10 within the negatively linear component of the graph (between 17°C and 27°C) generated a value of 0.24, accentuating this negative thermal dependence. Decreasing temperature also significantly increased both rise and decay time kinetics, while increasing temperature resulted in reduced kinetics (Figure 5C-D; 5C: one-way ANOVA, $P<0.0001$, N=12–18; 5D: $P<0.0001$, N=12–18). As described earlier, greater plasticity in muscle performance is observed between 20 and 30 Hz nerve stimulation. Consequently, this experiment was repeated with 25 Hz to determine if temperature had a more profound effect at a lower stimulation frequency. Significant differences were observed at 15, 16, 19, and 20°C, indicating more substantial effects of temperature at lower stimulation frequencies (Figure 5E; one-way ANOVA, $P<0.0001$, N=8–14). Rearing animals at different temperatures, particularly ectothermic animals, has been shown to adapt various aspect of an animal's physiology, shifting their physiological efficiency closer to rearing temperatures (Bennett, 1985). Thus, animals were reared at 22, 25 and 29°C to determine if muscle performance could be shifted rightward towards better performance at higher temperatures. No difference was observed in animals reared at distinct temperatures (Figure 5F), suggesting the muscle excitation-contraction machinery does not display temperature adaptation.

External calcium and magnesium concentration regulate muscle contraction

It is well established that both external Ca^{2+} and Mg^{2+} have a profound effect on pre-and post-synaptic intracellular mechanisms that contribute to muscle force production (Jan and Jan, 1976). Two commonly used *Drosophila* salines, hemolymph-like saline 3 and 3.1 (HL3 and HL3.1, Macleod et al, 2002), which contain 20 mM and 4 mM external Mg^{2+} respectively, were used to determine the effects of Mg^{2+} on force production. Additionally, 7 different external Ca^{2+} concentrations ($[Ca^{2+}]_o$) were explored for each saline, along with 4 different force-frequency stimulations durations (200, 300, 600, and 900 ms, Figure 6 & Figure 7). At 0.1 mM $[Ca^{2+}]_o$, the highest frequency stimulation (150 Hz) at the longest examined duration (900 ms) was unable to induce a recordable contraction in HL3. In contrast, a detectable contraction was observed at 10 Hz stimulation in HL3.1 (Figure 6A). Omitting external $[Ca^{2+}]$ resulted in no muscle contraction in either saline, even at the highest stimulation frequencies. Raising $[Ca^{2+}]_o$ from 0.1 to 0.25 mM was sufficient to induce contractions at higher stimulation frequencies and durations (40–150 Hz) in HL3 saline, although a profound difference remained between the two salines (Figure 6A). Figure 5B shows the effect of external Ca^{2+} and Mg^{2+} on the half-maximal (50%) stimulation frequency across the entire data set. Plotting the maximal force generated at each $[Ca^{2+}]_o$ for each stimulus duration generated data similar to that observed in Table 1, where an increase in either factor resulted in enhanced force generation in HL3. No differences between the total force generated was observed between the two salines above 1.0 mM $[Ca^{2+}]_o$ (Figure 6A, Figure 7). As such, the higher Mg^{2+} concentrations found in HL3 saline resulted in a

robust reduction in muscle contractile force, consistent with elevated Mg^{2+} reducing Ca^{2+} entry into the presynaptic terminal.

To determine if the magnitude of contractions elicited from a single stimulus represented a sensitive read-out of synaptic activity, we compared data obtained from single stimuli to that from stronger stimulations. The size of single-stimulus induced contractions as a percentage of force at 150 Hz stimulation was unchanged across stimulus durations (Table 1). The amplitude of contractions induced from a single stimulus increased in a proportional manner with increases in external Ca^{2+} and saturated beyond 1.5 mM in HL3.1 saline. While contractions elicited from single stimuli were not observed in HL3 saline until 1.0 mM $[Ca^{2+}]_o$, they increased proportionally from 1.0 to 2.0 mM $[Ca^{2+}]_o$ (Figure 6C-D). Similar proportionate increases in muscle excitability was observed in EJP recordings at the NMJ in HL3.1 saline (Figure 6E). These findings indicate contractions elicited from single stimuli, in addition to maximal force output, represent a robust mechanism to correlate synaptic function with the ECC machinery.

Synaptic and muscle Ca^{2+} channels strongly regulate muscle contraction amplitude

To further examine the role of Ca^{2+} in regulation of ECC at the *Drosophila* NMJ, pharmacological and genetic approaches were used to manipulate Ca^{2+} channel function. Voltage-gated Ca^{2+} channels play critical roles in synaptic transmission, providing the trigger for regulated neurotransmitter release and activation of the muscle actin-myosin contractile machinery. L-type Ca^{2+} channels found in muscle are essential for ECC in cardiac, smooth, and skeletal muscle cells (Beam, Tanabe and Numa, 1989; Franzini-Armstrong and Protasi, 1997) and are selectively antagonized by dihydropyridines such as felodipine. To examine how disruption of L-type Ca^{2+} channel function altered ECC, dose-dependent effects of felodipine application on the amplitude and rise- and decay-time kinetics of muscle contraction force were determined (Figure 8A). At 1 μM, felodipine had no significant effect on amplitude or contraction kinetics. However, 10 and 100 μM significantly reduced the amplitude of contractions (Figure 8A, one-way ANOVA, $P<0.0001$, N=5–7). At 1 and 10 μM, felodipine had no effect on the time course of contractions, though 100 μM felodipine application significantly increased both the rise- and decay-tau values (Figure 8A, one-way ANOVA, $P<0.0001$, N=5–7). As such, disruption of L-type Ca^{2+} channel function impacts both overall contractile force and contraction kinetics. The N-type Ca^{2+} channel Cacophony (Cac) localizes presynaptically at active zones and mediates voltage-dependent Ca^{2+} influx that drives synaptic vesicle fusion. To explore its role in muscle contractile properties, the GAL4/UAS system was used to express RNAi against Cac in motoneurons using a neuronal specific GAL4 driver (*elav*-GAL4). Knockdown of Cac dramatically reduced contractile force, but had no effect on contraction dynamics (Figure 8B, C, one-way ANOVA, $P<0.0001$, N=4–7). At 40 Hz stimulation, a 50.9% reduction in contraction force was observed compared to controls (Figure 8B). Addition of 10 μM felodipine to reduce L-type channel function in Cac RNAi larvae resulted in a 79.5% decrease in contractile force compared to controls, revealing a synergistic interaction following reduction in both channel subtypes (Figure 8C). No effects on contraction kinetics were observed under these conditions, suggesting contractile force is more sensitive to decreased Ca^{2+} influx.

Altering sarcoplasmic reticulum Ca^{2+} *cycling impacts muscle contraction amplitude and kinetics*

To examine the role of intracellular Ca^{2+} in regulating ECC, a pharmacological approach was taken to disrupt Ca^{2+} liberation from intracellular stores and Ca^{2+} exchange at the plasma membrane. The Ca^{2+}-dependent muscle contraction machinery is largely driven via release of Ca^{2+} from internal stores via the ryanodine receptor present in the sarcoplasmic reticulum (SR). Once Ca^{2+}-induced Ca^{2+}-release occurs, Ca^{2+} is actively pumped back into the SR via the sarcoplasmic/endoplasmic reticulum Ca^{2+} ATPase (SERCA) pump. Ca^{2+} liberation from the SR can be impaired using the non-competitive SERCA pump inhibitor thapsigargin. Dose-dependent effects of thapsigargin on muscle contraction amplitude and kinetics are shown in Figure 9A. Disruption of SERCA function affected both the force and kinetics of contraction, with significant increases in both rise- and decay-tau values (Figure 9A, one-way ANOVA, $P<0.0001$, N=5–7). To examine the role of intracellular SR Ca^{2+} liberation through ryanodine receptors, exogenous application of caffeine, well-known to activate ryanodine receptors, was used. Application of caffeine significantly decreased the amplitude of muscle contractions while increasing both the rise- and decay-time kinetics (Figure 9B, one-way ANOVA, $P<0.0001$, N=4–5). Ryanodine was also applied to larval preparations, where it potently decreased the amplitude of contractions, causing a 41.7 and 82.8% reduction at 0.01 and 0.1 μM respectively (Figure 9C; one-way ANOVA, $P<0.0001$, N=5–6). Ryanodine application also increased the decay-tau value in a dose-dependent manner, but had no effect on rise-time kinetics (Figure 9C). To reduce ryanodine receptor function, the GAL4/UAS system was used to knockdown the gene with the muscle-specific driver *mef2*-GAL4. As shown in Figure 9D, a substantial reduction in muscle force production was observed at each stimulation frequency in the force-frequency curve, with a 47.5% decrease in force at 40 Hz.

Neuromodulation at the Drosophila NMJ

To further explore pathways that may regulate ECC at the *Drosophila* NMJ, several classical neuromodulators and neurotransmitters shown to affect muscle performance in other systems were assayed. To initially screen these neuromodulators, a paradigm using steady-state 40 Hz stimulation for 600 ms with an interburst duration of 15 s was used as this stimulation generates robust muscle contractions but is below force saturation. Candidate neuromodulators were perfused onto larval preparations for 5 mins at the relatively high concentration of 10^{-5} M or 10^{-6} M so any potential effects on contraction could be detected. Several neuromodulators failed to show any effect on steady-state muscle contraction force during stimulation, including 10^{-5} M leucokinin, 10^{-5} M gamma-aminobutyric acid (GABA), 10^{-5} M acetylcholine, 10^{-5} M pituitary adenylate cyclase activating polypeptide (PACAP27), 10^{-5} M histamine, and 10^{-5} M dopamine (Figure 10A-F). In contrast, the TPAEDFMRFa peptide encoded by the *FMRFa* gene previously implicated in muscle performance robustly enhanced muscle contraction force (Hewes *et al.,* 1998). Exogenous application of 10^{-6} M TPAEDFMRFa steadily increased amplitude of muscle contraction, reaching a maximal effect after 5 min of perfusion that resulted in an average force increase of 29 ± 6.4% (Figure 10G). A dose-response curve for enhanced muscle contractile force was generated by examining the effects of TPAEDFMRFa at 10^{-5} M, 10^{-6} M, 10^{-7} M, 10^{-8} M, 10^{-9} M, and 10^{-10} M with 7 replicate animals for each concentration (Figure 10H).

Under these conditions, the [EC_{50}] of TPAEDFMRFa for enhancing muscle contraction was 5.38×10^{-8} M (Figure 10H).

To further characterize this neuromodulator, the same series of TPAEDFMRFa concentrations were applied using a dynamic force-frequency curve paradigm. Control recordings were conducted by running larvae through the stimulation protocol from 1–150 Hz, waiting a period of 5 min, then performing the same stimulation protocol a 2nd time. For experimental trials, the neuropeptide was perfused in during the 5 min rest period between trials and throughout the entirety of the 2nd stimulation period. The effects of TPAEDFMRFa on muscle force across each frequency and at each concentration are summarized in Figure 10I. At 40 Hz, the [EC_{50}] was 2.1×10^{-8} M using the dynamic protocol (Figure 10H). There were no statistical differences between TPAEDFMRFa concentrations at 100 and 150 Hz stimulation, although significant increases were observed at 50 Hz stimulation from 10^{-7} to 10^{-5} M (one-way ANOVA, $P<0.0001$, N=4–7). Surprisingly, stimulation frequency decreases contraction efficiency as TPAEDFMRFa concentration increases, peaking at 5 Hz where a nearly 200% increase in contraction force is observed at 10^{-5} and 10^{-6} M. Based on control conditions (Figure 2), we predicted that the peptide would exert the greatest effect between stimulation frequencies of 20 to 35 Hz where the contractile machinery is most sensitive to nerve output. In contrast, the effectiveness of the peptide increased as stimulation frequency decreased. EC_{50} values generated for each stimulation frequency revealed similar values in the 2.1 to 3.9×10^{-8} M range.

To begin elucidating the molecular pathway by which TPAEDFMRFa exerts its effects on contraction force, the UAS-GAL4 system was employed to knockdown the FMRFa receptor using UAS-RNAi against *FMRFa* mRNA. The pan-neuronal driver elav-GAL4 was used to express *FMRFa* RNAi presynaptically in motoneurons and the muscle specific mef2-GAL4 was used to drive RNAi postsynaptically in muscles. Knockdown of the FMRFa receptor either preor post-synaptically significantly reduced the ability of TPAEDFMRFa to enhance muscle contraction force (Figure 11A, One-way ANOVA, $P<0.0001$, N=4–6). Using both GAl4 drivers to simultaneously knockdown the FMRFa receptor pre- and post-synaptically resulted in an additive decrease in the ability of the peptide to enhance contraction. However, TPAEDFMRFa was still able to partially increase contraction even when the FMRFa receptor was knocked down simultaneously with both drivers. In addition to the FMRFa receptor, myosuppressin receptors have also been shown to mediate some behavioral effects for a different FMRFa peptide, DPKQDFMRFa (Klose *et al.,* 2010). To determine if TPAEDFMRFa might also activate this pathway, the two myosuppressin receptors encoded in the genome were targeted with independent RNAi lines to assay their involvement in TPAEDFMRF's ability to enhance muscle contraction. Pre- and post-synaptic expression of RNAi against the Dromyosuppressin receptor 1 did not significantly reduce the ability of the peptide to potentiate muscle contraction (Figure 11B, One-way ANOVA, $P<0.0001$, N=4–7). However, knockdown of Dromyosuppressin receptor 2 with either *mef2*-GAL4 or with both *mef2*-GAL4 and *elav*-GAL4 simultaneously significantly reduced the ability of TPAEDFMRFa to potentiate muscle contraction force (Figure 11B, One-way ANOVA, $P=0.0955$, N=4–7). Taken together, these results indicate the TPAEDFMRFa neuropeptide

enhances muscle contractions through activity in both pre- and post-synaptic compartments via the FMRFa receptor and Dromyosuppressin receptor 2.

Discussion

These findings indicate the excitation-contraction coupling machinery in *Drosophila* larvae provides a valuable system for exploring and dissecting the component parts that contribute to and regulate neuromotor circuitry underlying ECC. Using a force transducer with 10 μN resolution, the contribution of key biophysical, physiological, genetic and molecular parameters to muscle contractility was assayed. These data indicate neither the size of 3rd instar larvae nor the muscle subgroup examined had any significant effect on maximal force production or biophysical properties of ECC across the whole animal (Figure 3). Although muscle architecture can impact force production (Burkholder *et al.,* 1994; David *et al.,* 2016), previous studies have shown that muscle length does not result in greater force production (Forman, Ford and Sonnenblick, 1972). Comprised mainly of chitinous bundles (microtubules), the cuticle must also contract and deform along with muscle fibers. The majority of cuticle fibers run parallel to the longitudinal axis of the larval, or anisotropic, and are structurally aligned with muscles underlying peristalsis (Tajiri *et al.,* 2017). Although we did not examine the role of the cuticle in anchoring bodywall muscles, the cuticle is a more rigid structure that requires additional force for deformation that may filter forces generated by the underlying bodywall muscles (Petzold *et al.,* 2011).” As descending information from the CNS via the locomotory CPG largely determines muscle performance, our examination of the role of stimulation duration and frequency yielded several critical observations. All stimulation durations displayed a sigmoidal relationship between force generation and stimulation frequency. Force generation saturated at/above 100 Hz stimulation and 200 ms stimulus duration. Beyond this, the muscle remains in a state of static-tension also referred to as catch-tension (Hoyle, 1984). Below 100 Hz stimulation frequency, force-frequency curves show considerable muscle plasticity. At some stimulus frequencies muscle force can vary by over 80% by altering stimulus duration. Thus, the combination of super-contractile bodywall muscles with a highly variable locomotor CPG provides the system with capacity for modulation and plasticity of muscle performance.

The highly variable nature of endogenous locomotory contractions was observed by performing force recordings in larvae with an intact CNS. The duration of fictive contractions ranged from <1 s to 25 s and generated forces from 0.2 mN to 7.4 mN. Interburst durations also revealed considerable duration between fictive bursts, although more than 50 percent of contractions occurred with no delay. Some endogenous contractions were multicomponent, comprised of multiple-peaks before returning to baseline. A typical intracellular voltage recording from larval bodywall muscles with the CNS intact showed intraburst EJP frequencies that reflect a parabolic shape going from low-high-low, which is unlikely to result in the generation of multiple peaks within a single contraction (Weiss *et al.,* 2019). This likely reflects non-synchronous contractions of different abdominal hemi-segments, with a lack of synchrony between abdominal segments due to loss of feedback from the peripheral nervous system in the dissected preparation (Caldwell *et al.,* 2003; Song *et al.,* 2007). We estimated the endogenous stimulation frequency of single component fictive contractions (Figure 4E) using force-frequency curves generated in Figure 2. Average

endogenous contractions are predicted to be elicited at 20–30 Hz motor neuron spiking, suggesting the CPG operates within the range of greatest plasticity.

Changes in external Mg^{2+} and Ca^{2+} have a profound effect on neurotransmitter release (Katz and Miledi, 1970; Hille, 1985; Augustine, Charlton and Smith, 1987). Increases in $[Ca^{2+}]_o$ at the *Drosophila* NMJ have a sigmoidal relationship with excitatory junctional currents, saturating at ~1.0 mM (Rohrbough *et al.,* 1999; Roche *et al.,* 2002). Figure 6E reveals a similar effect on EJPs, saturating at 1.0mM, which was also observed for muscle force production, showing a sigmoidal curve saturating at 1.0 mM external Ca^{2+} in *Drosophila* HL3.1 saline from single AP induced contractions (Figure 6D). These experiments also demonstrated that single AP induced contractions can serve as a viable parallel for traditional examinations of synaptic physiology, and illuminate how specific molecular and structural components impact not only postsynaptic depolarization (current or voltage recordings) but also direct contraction coupling. Increasing the external Mg^{2+} concentration from 4 mM to 20 mM also causes significant effects on contraction. At low external Ca^{2+} concentrations (0.1 mM), contractions were not observed at any stimulation frequency or duration with 20 mM Mg^{2+}, compared to robust contractions observed in 4 mM Mg^{2+} (Fig 6A). A significant decrease in muscle force production was apparent in 0.25 and 0.5 mM $[Ca^{2+}]_o$ in 4 mM vs. 20 mM $[Mg^{2+}]_o$. Consequently, saline composition is a critical factor to consider in experimental design. HL3.1 saline is desirable for contraction recordings as it generates robust contractions at low $[Ca^{2+}]$o, and has a more dynamic working range than HL3 (Figure 5 B). Taken together, the effects of external Ca^{2+} on synaptic physiology appear to couple in a 1:1 fashion with the contraction machinery. These effects of Mg^{2+} may be a consequence of presynaptic effects on Ca^{2+} channels or secondary effects on the muscle contractile machinery.

The presynaptic voltage-gated Ca^{2+} channel al subunit cacophony, Cac, is a critical player in chemical synaptic transmission and provides the trigger for regulated neurotransmitter release (Lee, Ueda and Wu, 2014). Temperature-sensitive mutations in Cac reduce EJP amplitude by 60% at the *Drosophila* NMJ (Kawasaki, Collins and Ordway, 2002). Here we explored the role of Cac by reducing its expression using the UAS-GAL4 system to drive *Cac* RNAi in motor neurons. Across all 11 stimulation frequencies, Cac knockdown showed a 45% reduction in contraction on average, indicating reductions in EJP amplitude directly translates to an equivalent reduction in muscle force. Following neurotransmitter release, muscle-cell depolarization via activation of glutamate receptors activates dihydropyridine-sensitive L-type Ca^{2+} channels to facilitate Ca^{2+} entry into the muscle cell (Marrus *et al.,* 2004; Kuo and Ehrlich, 2015). We find that the L-type Ca^{2+} channel blocker, felodipine, greatly reduces contraction amplitude. The effects of felodipine did not affect muscle contraction time-course kinetics below 10 uM. However, at higher concentrations, the rise and decay kinetics was significantly increased and correlated with greatly reduced contraction amplitude (Figure 2). Adding felodipine to Cac RNAi knockdown animals showed an additive effect on amplitude, suggesting these two pathways are separate components of the ECC machinery. The lack of effect on rise/decay time constants suggests both act upstream of the muscle-contraction machinery.

Upon depolarization of muscle cells, L-type Ca^{2+} channel opening in t-tubules activates ryanodine receptors located in the SR membrane to liberate release from internal stores (Kuo and Ehrlich, 2015). The bulk of Ca^{2+} used during actin-myosin cross-bridge formation comes from internal stores (Cho *et al.,* 2017). To explore this pathway, pharmacological application of ryanodine, which holds the receptor in an open state and causes a steady loss of Ca^{2+} from the SR, resulted in a dose-dependent reduction on muscle contraction amplitude (Smith *et al.,* 1988). Ryanodine also triggered a dose-dependent, significant increase in decay tau. RNAi knockdown of the ryanodine receptor in muscle also resulted in an average 41% reduction in contractile force across the 11 stimulation frequencies. Chronically elevated intramuscular Ca^{2+} would prevent rapid Ca^{2}+ clearance and storage in the SR and cause continuous actin-myosin cross-bridge cycling, effectively keeping fibers in a sustained contractile state (Squire, 2019). Chronically open ryanodine receptors will also be unable to restore SR Ca^{2+} to sufficient levels and thereby lead to a reduction in amplitude of subsequent contractions (Kolstad *et al.,* 2018). The main mechanism of $[Ca^{2+}]_i$ homeostasis following release is active transport back into the SR via the thapsigargin-sensitive SERCA pump (MacLennan, 1990). We observed that thapsigargin decreased contraction amplitude in a dose-dependent manner, but also increased the rise- and decay-tau values, most likely as a result of chronically elevating intramuscular $[Ca^{2+}]$.

Previous work noted a gradual but significant reduction in the EJP amplitude with increases in temperature, ultimately resulting in the inability to elicit an EJP at 40–42°C (Y. Feng, Ueda and Wu, 2004). Our results demonstrate that increasing temperature also gradually and significantly decreases the force of muscle contraction, resulting in the inability to elicit contractions between 34 and 39°C (Fig. 4). Previously observed temperature-dependent effects on EJP amplitude correlate with the effects of temperature on muscle contraction dynamics observed here (Figure 5) (Yanfei Feng, Ueda and Wu, 2004). The strength of muscle contraction also increased with decreases in temperature, saturating at 17–18°C. While effects of temperature on synaptic efficacy appear to directly translate to the ECC machinery, temperature may also impact muscle biology.

ECC has been extensively investigated in model organisms, with classical work performed in arthropods. These studies have provided a foundation for understanding the major components and principles governing ECC. Studies in arthropod peripheral synapses have examined the mechanisms of quantal release (Dudel and Kuffler, 1961c), short-term facilitation (Dudel and Kuffler, 1961a), synaptic inhibition (Dudel and Kuffler, 1961b), long-term synaptic facilitation (Sherman and Atwood, 1971), neurotransmitter identification and characterization (Otsuka, Kravitz and Potter, 1967; Kawagoe, Onodera and Takeuchi, 1981), and neuromodulation (Kravitz *et al.,* 1980). Across the animal kingdom, structural and morphological examinations of NMJs have been conducted since the 1800s (Foettinger, 1880). Physiologically, the importance of Ca^{2+} in muscle contraction has been long known (Heilbrunn and Wiercinski, 1947), while the isolation of the SR and its role in Ca^{2+} storage decades were characterized later (Weber, Herz and Reiss, 1963; Weber and Hertz, 1968). The relationship between membrane voltage and tension and critical roles for key ions (e.x. Na^{+}, K^{+}, Cl^{-}) have also been described (Hodgkin and Horowicz, 1959b, 1959a; Reuben *et al.,* 1967). Major questions about depolarization-induced Ca^{2+}-release and the role of Ca^{2+} in activation of the main contractile machinery (actin and myosin) have also been

heavily investigated (Hagiwara and Nakajima, 1966; Ashley, 1967; Chiarandini *et al.,* 1970). Pharmacological agents influencing muscle contraction have long been of interest in the field (Putney and Biancri, 1974; Caputo, 1976). Many of the processes governing ECC are conserved in *Drosophila,* demonstrated here and elsewhere (Jan and Jan, 1976; Song *et al.,* 2007; Paterson, Anikin and Krans, 2010; Ormerod *et al.,* 2013; Singhania and Grueber, 2014; Hasegawa, Truman and Nose, 2016; K. G. Ormerod, Jung and Mercier, 2018).

The NMJ of arthropods have long been explored as critical areas of influence by neuromodulatory substances (Robbins, 1959; Van Harreveld and Mendelson, 1959). Among the small neuromodulators that have been shown to modulate muscle performance in multiple vertebrate and invertebrate model systems, we assayed muscle contraction force changes in the presence of dopamine, histamine, acetylcholine and GABA (Kravitz, Kuffler and Potter, 1963; Reite, 1972; Lingle, 1981; Cooper and Neckameyer, 1999; Picciotto, Higley and Mineur, 2012). No observable effect of these neuromodulators at the *Drosophila* glutamatergic NMJ were found. Multiple neuropeptides have also been suggested to modulate the neuromuscular system. Landgraf et al, (2003) described leucokinin-immunoreactivity in type III terminals at the *Drosophila* NMJ, but we found no effect on contraction when leucokinin was exogenously applied to the dissected larval preparation (Landgraf *et al.,* 2003). Pituitary adenylate cyclase activating polypeptide (PACAP) is encoded by the amnesiac gene in *Drosophila.* PACAP-38 has previously been shown to modulate Ca^{2+} channel dynamics and contraction in *Drosophila* 3rd instar bodywall muscles (Zhong and Peña, 1995; Bhattacharya, Lakhman and Singh, 2004). We found that the shorter isoform, PACAP-27, had no effect on muscle contraction. The *Drosophila* genome encodes a single gene for FMRF-like peptides which encodes 8 unique peptides. DPKQDFMRFa is the most abundant, with 5 replicate copies, and has been previously characterized in *Drosophila.* DPKQDFMRFa enhances synaptic transmission via the CaMKII pathway through the FMRFa receptor (Dunn and Mercier, 2003; Klose *et al.,* 2010). DPKQDFMRFa also increases nerve-evoked contractions and can also elicit contractions in the absence of the CNS (Hewes *et al.,* 1998; Clark *et al.,* 2008; Ormerod, Krans and Mercier, 2015).

The second most abundant FMRFa-like peptide is TPAEDFMRFa with two replicate copies (Nambu *et al.,* 1988; Taghert and Schneider, 1990). Previous work has shown that TPAEDFMRFa enhances twitch tension in a reduced preparation from *Drosophila* 3rd instar larvae in a similar magnitude to DPKQDFMRFa (Hewes *et al.,* 1998). To examine how this pathway modulates neuromuscular contraction, we tested the effects of exogenous application of TPAEDFMRFa by eliciting contractions using 40 Hz stimulation. This paradigm revealed a robust increase in the amplitude of nerve-evoked contractions that did not wash out with 10 min of saline perfusion at 10^{-6}M (Figure 9G), but did washout after 10 min at 10^{-7}M. TPAEDFMRFa displayed an EC_{50} of 5.4×10^{-8}M, generating a 20% increase in the amplitude of contractions to a maximal increase of 38% at 10^{-6}M. By examining the effects of the peptide across a wide-range of stimulation frequencies from 1–150 Hz, TPAEDFMRFa was much more effective at increasing contraction force at lower stimulation frequencies, with maximal effects observed at 5 and 10 Hz (189 ± 28% and 156 ± 10% respectively). The lack of modulation at higher stimulation frequencies is likely a result of muscle contraction being at or near saturation. Previous studies

in *Drosophila* revealed that the biogenic amine octopamine was also more effective at enhancing contractions at lower stimulation frequencies, while its precursor tyramine had no effects (Ormerod *et al.,* 2013). Similar to what was observed for TPAEDFMRFa, the greatest modulation was observed below 20 Hz. There are a multitude of mechanisms through which modulators have been shown to enhance contractile force, namely via second messenger pathways to promote Ca^{2+} liberation from internal stores (Kuo and Ehrlich, 2015) However, more recent studies provide evidence for functional modification of elastic proteins within muscles that may give them greater capacity for force production, even at lower stimulation frequencies when modified or phosphorylated (Herwig *et al.,* 2020). Nevertheless, release of neuromodulatory substances like FMRFa peptides or biogenic amines like octopamine would maximize the amplitude of contractions, enabling larvae to generate a stronger contraction with less synaptic input. Interestingly, octopamine profoundly increases the basal tension of larval muscle fibers, while FMRFa-like peptides have comparatively little effect (Clark *et al.,* 2008; Ormerod *et al.,* 2013; Milakovic *et al.,* 2014) Release of peptides or biogenic amines could aid in the fight-or-flight response to enable larvae to reach maximal locomotor velocity or play a role in preventing synaptic fatigue under conditions of chronic neuromotor activation.

Using the UAS/GAL4-system, the FMRFa receptor was found to be required in both pre- and postsynaptic compartments to potentiate nerve-evoked contractions. However, using nerve and muscle-specific drivers simultaneously was insufficient to completely abolish the effect on contraction force. It is therefore likely that other receptors also contribute to the enhancement of nerve-evoked contractions by the peptide. We tested knockdown of two myosuppressin receptors previously implicated in mediating the effects of DPKQDFMRFa (Klose *et al.,* 2010). Myosuppressin receptor 1 appears to play no role in the enhancement of nerve-evoked contractions by TPAEDFMRFa. Knocking down myosuppressin receptor 2 either postsynaptically, or pre and post-synaptically, significantly reduced the ability of the peptide to enhance contraction. Ca^{2}+ imaging studies using DPKQDFMRFa revealed a strong presynaptic enhancement following peptide application in motoneuron Ib boutons (Klose *et al.,* 2010). Ormerod et al, (2015) demonstrated that the FMRFa receptor is expressed in muscle fibers 4, 6, 7, 12, and 13, the muscles which produce the bulk of ventral force during larval peristalsis. Thus, the FMRFa receptor is expressed and functional presynaptically, as well as in bodywall muscles. Future studies will be required to precisely define the ability of these peptides to selectively recruit neurons and other effectors.

Taken together, these results demonstrate that *Drosophila* provides as a robust system to characterize excitation-contraction coupling. Analysis of the force-frequency components of contraction described here indicate *Drosophila* muscle contractile force is similar to force-frequency data described in vertebrate models (Terry, Kaneb and Wells, 2014; Eshima *et al.,* 2017). Indeed, critical muscle genes underlying the development and function of the musculature are highly conserved between *Drosophila* and vertebrates (Taylor, 2013). As such, *Drosophila* larval bodywall muscles provide an excellent model for investigation of excitation-contraction coupling and linking known synaptic defects in neuronal mutants to their final effect on muscle force production.

References

Aponte-Santiago NA et al. (2020) 'Synaptic Plasticity Induced by Differential Manipulation of Tonic and Phasic Motoneurons in Drosophila The Journal of Neuroscience. Society for Neuroscience, 40(33), pp. 6270–6288. doi: 10.1523/jneurosci.0925-20.2020.

Ashley C. (1967) 'The role of cell calcium in the contraction of single cannulated muscle fibers', American zoologist. Am Zool, 7(3), pp. 647–659. doi: 10.1093/ICB/7.3.647. [PubMed: 6077383]

Atwood HL (1967) 'Crustacean Neuromuscular Mechanisms', 7, pp. 527–551. Available at: https://academic.oup.com/icb/article/7/3/527/245393 (Accessed: 20 September 2021).

Augustine GJ, Charlton MP and Smith SJ (1987) Cacium action in synaptic transmitter release. Available at: www.annualreviews.org (Accessed: 5 February 2020).

Beam KG, Tanabe T. and Numa S. (1989) 'Structure, Function, and Regulation of the Skeletal Muscle Dihydropyridine Receptor', Annals of the New York Academy of Sciences, 560(1), pp. 127–137.doi:10.1111/j.1749-6632.1989.tb24090.x. [PubMed: 2545129]

Belanger JH (2005) 'Contrasting Tactics in Motor Control by Vertebrates and Arthropods 1', 45, pp. 672–678. Available at: https://academic.oup.com/icb/article/45/4/672/636447 (Accessed: 20 September 2021).

Bennett AF (1985) 'Temperature and muscle', Journal of Experimental Biology, 115(1).

Bhattacharya A, Lakhman SS and Singh S. (2004) 'Modulation ofL-type calcium channels in Drosophila via a pituitary adenylyl cyclase-activating polypeptide (PACAP)-mediated pathway', Journal of Biological Chemistry, 279(36), pp. 37291–37297. doi: 10.1074/jbc.M403819200.

Budnik V. (1996) 'Synapse maturation and structural plasticity at Drosophila neuromuscular junctions.', Current opinion in neurobiology, 6(6), pp. 858–67. doi: 10.1016/s0959-4388(96)80038-9. [PubMed: 9000022]

Burkholder TJ et al. (1994) Relationship Between Muscle Fiber Types and Sizes and Muscle Architectural Properties in the Mouse Hindlimb, JOURNAL OF MORPHOLOGY.

Caldwell JC et al. (2003) 'Dynamic analysis of larval locomotion in Drosophila chordotonal organ mutants.', Proceedings of the National Academy of Sciences of the United States of America, 100(26), pp. 16053–8. doi: 10.1073/pnas.2535546100. [PubMed: 14673076]

Caputo C. (1976) 'The effect of caffeine and tetracaine on the time course of potassium contractures of single muscle fibres', The Journal of physiology. J Physiol, 255(1), pp. 191–207. doi:10.1113/JPHYSI0L.1976.SP011275. [PubMed: 1082935]

Cheng LE et al. (2010) 'The role of the TRP channel NompC in Drosophila larval and adult locomotion.', Neuron, 67(3), pp. 373–80. doi: 10.1016/j.neuron.2010.07.004. [PubMed: 20696376]

Chiarandini DJ et al. (1970) 'Effects of Caffeine on Crayfish Muscle Fibers I. Activation of contraction and induction of Ca spike electrogenesis', Journal of General Physiology. The Rockefeller University Press, 55(5), pp. 640–664. doi: 10.1085/JGP.55.5.640.

Cho CH et al. (2017) 'A focus on extracellular Ca2+ entry into skeletal muscle', Experimental and Molecular Medicine. Nature Publishing Group, p. 378. doi: 10.1038/emm.2017.208.

Clark J. et al. (2008) 'Evidence for postsynaptic modulation of muscle contraction by a Drosophila neuropeptide.', Peptides, 29(7), pp. 1140–9. doi: 10.1016/j.peptides.2008.02.013. [PubMed: 18394755]

Clark MQ et al. (2018) 'Neural circuits driving larval locomotion in Drosophila', Neural Development. BioMed Central Ltd. doi: 10.1186/s13064-018-0103-z.

Cooper RL and Neckameyer WS (1999) 'Dopaminergic modulation of motor neuron activity and neuromuscular function in Drosophila melanogaster.', Comparative biochemistry and physiology. Part B, Biochemistry & molecular biology, 122(2), pp. 199–210. doi: 10.1016/s0305-0491(98)10160-8. [PubMed: 10327610]

David S. et al. (2016) 'Musculoskeletal modelling under an evolutionary perspective: Deciphering the role of single muscle regions in closely related insects', Journal of the Royal Society Interface. Royal Society of London, 13(123). doi: 10.1098/rsif.2016.0675.

Dudel J. and Kuffler S. (1961a) ‘Mechanism of facilitation at the crayfish neuromuscularjunction’, The Journal of physiology. J Physiol, 155(3), pp. 530–542. doi: 10.1113/JPHYSIOL.1961.SP006645. [PubMed: 13724751]

Dudel J. and Kuffler S. (1961b) ‘Presynaptic inhibition atthe crayfish neuromuscularjunction’, The Journal of physiology. J Physiol, 155(3), pp. 543–562. doi: 10.1113/JPHYSIOL.1961.SP006646. [PubMed: 13724752]

Dudel J. and Kuffler S. (1961c) ‘The quantal nature of transmission and spontaneous miniature potentials at the crayfish neuromuscularjunction’, The Journal ofphysiology. J Physiol, 155(3), pp. 514–529. doi:10.1113/JPHYSIOL.1961.SP006644. [PubMed: 13724753]

Dunn TW and Mercier AJ (2003) ‘Synaptic modulation by a neuropeptide depends on temperature and extracellular calcium’, Journal of Neurophysiology. J Neurophysiol, 89(4), pp. 1807–1814. doi:10.1152/jn.00710.2002. [PubMed: 12686567]

Eshima H. et al. (2017) ‘Long-term, but not short-term high-fat diet induces fiber composition changes and impaired contractile force in mouse fast-twitch skeletal muscle’, Physiological Reports. American Physiological Society, 5(7), p. e13250. doi: 10.14814/phy2.13250.

Feng Y, Ueda A. and Wu C-F (2004) ‘A modified minimal hemolymph-like solution, HL3.1, for physiological recordings at the neuromuscularjunctions of normal and mutant drosophila larvae’, Journal of Neurogenetics, 18(2), pp. 377–402. doi: 10.1080/01677060490894522. [PubMed: 15763995]

Feng Yanfei, Ueda, A. and Wu, C. F. (2004) ‘A modified minimal hemolymph-like solution, HL3.1, for physiological recordings at the neuromuscularjunctions of normal and mutant Drosophila larvae’, Journal of Neurogenetics, 18(2), pp. 377–402. doi: 10.1080/01677060490894522. [PubMed: 15763995]

Foettinger A. (1880) ‘Sur le terminaison des nerfs dans les muscles des insectes’, Arch. Biol, (1), pp. 279–304.

Forman R, Ford LE and Sonnenblick EH (1972) Effect of Muscle Length on the Force-Velocity Relationship of Tetanized Cardiac Muscle, Circulation Riittreb. Available at: http://ahajournals.org (Accessed: 5 February 2020).

Fox LE, Soll DR and Wu C-F (2006) ‘Coordination and modulation oflocomotion pattern generators in Drosophila larvae: effects of altered biogenic amine levels by the tyramine beta hydroxylase mutation.’, The Journal of neuroscience : the officialjournal of the SocietyforNeuroscience, 26(5), pp. 1486–98. doi: 10.1523/JNEUR0SCI.4749-05.2006.

Franzini-Armstrong C. and Protasi F. (1997) Ryanodine Receptors of Striated Muscles: a Complex Channel Capable of Multiple Interactions, REVIEWS.

Goulding M. (2009) ‘Circuits controlling vertebrate locomotion: Moving in a new direction’, Nature Reviews Neuroscience, pp. 507–518. doi: 10.1038/nm2608. [PubMed: 19543221]

Hagiwara S. and Nakajima S. (1966) ‘Effects of the intracellular Ca ion concentration upon the excitability of the muscle fiber membrane of a barnacle’, The Journal of general physiology. J Gen Physiol, 49(4), pp. 807–818. doi: 10.1085/JGP.49.4.807. [PubMed: 5943616]

Van Harreveld A. and Mendelson M. (1959) ‘Glutamate-induced contractions in crustacean muscle.’, Journal of cellular and comparative physiology, 54, pp. 85–94. doi: 10.1002/jcp.1030540109. [PubMed: 13841073]

Harris KP and Littleton JT (2015) ‘Transmission, development, and plasticity of synapses’, Genetics. Genetics, 201(2), pp. 345–375. doi: 10.1534/genetics.115.176529.

Hasegawa E, Truman JW and Nose A. (2016) ‘Identification of excitatory premotor intemeurons which regulate local muscle contraction during Drosophila larval locomotion’, Scientific Reports. Nature Publishing Group, 6. doi: 10.1038/srep30806.

Heckscher ES, Lockery SR and Doe CQ (2012) ‘Characterization ofDrosophila larval crawling at the level of organism, segment, and somatic body wall musculature’, Journal of Neuroscience, 32(36), pp. 12460–12471. doi: 10.1523/JNEUR0SCI.0222-12.2012. [PubMed: 22956837]

Heilbrunn L. and Wiercinski F. (1947) ‘The action of various cations on muscle protoplasm’, Journal of cellular and comparative physiology. J Cell Comp Physiol, 29(1), pp. 15–32. doi:10.1002/JCP.1030290103. [PubMed: 20285919]

Herwig M. et al. (2020) ‘Modulation ofTitin-Based Stiffness in Hypertrophic Cardiomyopathy via Protein Kinase D’, Frontiers in Physiology. Frontiers, 0, p. 240. doi: 10.3389/FPHYS.2020.00240.

Hewes RS et al. (1998) ‘Functional redundancy of FMRFamide-related peptides at the Drosophila larval neuromuscularjunction’, Journal of Neuroscience. Society for Neuroscience, 18(18), pp. 7138–7151. doi: 10.1523/jneurosci.18-18-07138.1998. [PubMed: 9736637]

Hille B. (1985) ‘Ionic channels of excitable membranes. Bertil Hille. Sunderland, Ma: Sinauer Associates, 1984’, Journal of Neuroscience Research, 13(4), pp. 599–600. doi: 10.1002/jnr.490130415.

Hoang B. and Chiba A. (2001) ‘Single-cell analysis ofDrosophila larval neuromuscular synapses’, Developmental Biology. Academic Press Inc, 229(1), pp. 55–70. doi: 10.1006/dbio.2000.9983.

Hodgkin AL and Horowicz P. (1959a) ‘Movements ofNa and K in single muscle fibres’, The Journal of Physiology. Wiley-Blackwell, 145(2), p. 405. doi: 10.1113/JPHYSI0L.1959.SP006150. [PubMed: 13642309]

Hodgkin AL and Horowicz P. (1959b) ‘The influence of potassium and chloride ions on the membrane potential of single muscle fibres’, The Journal of Physiology. Wiley-Blackwell, 148(1), p. 127. doi:10.1113/JPHYSI0L.1959.SP006278. [PubMed: 14402240]

Hoyle G. (1983) Muscles and their neural control. Edited by N. Y. Wiley Interscience. Wiley.

Hoyle G. (1984) ‘Neuromusculartransmission in aprimitive insect: Modulation by octopamine, and catch-like tension’, Comparative Biochemistry and Physiology. Part C, Comparative. Comp Biochem Physiol C Comp Pharmacol Toxicol, 77(2), pp. 219–232. doi: 10.1016/0742-8413(84)90005-7.

Hughes CL and Thomas JB (2007) ‘A sensory feedback circuit coordinates muscle activity in Drosophila.’, Molecular and cellular neurosciences, 35(2), pp. 383–96. doi: 10.1016/j.mcn.2007.04.001.

Jan LY and Jan YN (1976) ‘Properties of the larval neuromuscularjunction in Drosophila melanogaster.’, The Journal of physiology, 262(1), pp. 189–214. Available at: http://www.ncbi.nlm.nih.gov/pubmed/11339 (Accessed: 16 August 2016). [PubMed: 11339]

Katz B. and Miledi R. (1970) ‘Further study of the role of calcium in synaptic transmission’, The Journal of Physiology, 207(3), pp. 789–801. doi: 10.1113/jphysiol.1970.sp009095. [PubMed: 5499746]

Katz PS and Frost WN (1995) ‘Intrinsic neuromodulation in the Tritonia swim CPG: Serotonin mediates both neuromodulation and neurotransmission by the dorsal swim intemeurons’, Journal of Neurophysiology. American Physiological Society, 74(6), pp. 2281–2294. doi:10.1152/jn.1995.74.6.2281. [PubMed: 8747191]

Kawagoe R, Onodera K. and Takeuchi A. (1981) ‘Release of glutamate from the crayfish neuromuscularjunction’, The Journal of physiology. J Physiol, 312(1), pp. 225–236. doi: 10.1113/JPHYSIOL.1981.SP013625. [PubMed: 7264992]

Kawasaki F, Collins SC and Ordway RW (2002) ‘Synaptic calcium-channel function in Drosophila: Analysis and transformation rescue of temperature-sensitive paralytic and lethal mutations of Cacophony’, Journal of Neuroscience. Society for Neuroscience, 22(14), pp. 5856–5864. doi:10.1523/jneurosci.22-14-05856.2002. [PubMed: 12122048]

Keshishian H. et al. (1996a) ‘The drosophila neuromuscularjunction: a model system for studying synaptic development and function.’, Annual review of neuroscience, 19(1), pp. 545–75. doi:10.1146/annurev.ne.19.030196.002553.

Keshishian H. et al. (1996b) ‘The DrosophilaNeuromuscular Junction: A Model System for Studying Synaptic Development and Function’, Annual Review of Neuroscience, 19(1), pp. 545–575. doi:10.1146/annurev.ne.19.030196.002553.

Klose MK et al. (2010) ‘Peptide-induced modulation of synaptic transmission and escape response in Drosophila requires two G-protein-coupled receptors’, Journal of Neuroscience. J Neurosci, 30(44), pp.14724–14734. doi: 10.1523/JNEUROSCI.3612-10.2010. [PubMed: 21048131]

Koh YH, Gramates LS and Budnik V. (2000) ‘Drosophila larval neuromuscularjunction: Molecular components and mechanisms underlying synaptic plasticity’\ Microscopy Research and Technique, 49(1), pp. 14–25. doi: 10.1002/(SICI)1097-0029(20000401)49:1<14::AID-JEMT3>3.0.CO;2-G.

Kolstad TR et al. (2018) 'Ryanodine receptor dispersion disrupts Ca 2+ release in failing cardiac myocytes', eLife. eLife Sciences Publications Ltd, 7. doi: 10.7554/eLife.39427.

Kravitz E. et al. (1980) 'Amines and a Peptide as Neurohormones in Lobsters: Actions on Neuromuscular Preparations and Preliminary Behavioural Studies', Journal of Experimental Biology. The Company of Biologists, 89(1), pp. 159–175. doi: 10.1242/JEB.89.1.159.

Kravitz EA, Kuffler SW and Potter DD (1963) 'Gamma-aminobutyric acid and other blocking compounds in crustacea III. Their relative concentrations in separated motor and inhitory axons', Journal of neurophysiology, 26, pp. 739–751. doi: 10.1152/jn.1963.26.5.739. [PubMed: 14065325]

Kuo IY and Ehrlich BE (2015) 'Signaling in muscle contraction', Cold Spring Harbor Perspectives in Biology. Cold Spring Harbor Laboratory Press, 7(2). doi: 10.1101/cshperspect.a006023.

Landgraf M. et al. (2003) 'Charting the Drosophila neuropile: A strategy for the standardised characterisation of genetically amenable neurites', *Developmental Biology.* Academic Press Inc., 260(1),

Lee J, Ueda A. and Wu CF (2014) 'Distinct roles ofDrosophila cacophony and DmcalD Ca2+ channels in synaptic homeostasis: Genetic interactions with slowpoke Ca2+-activated BK channels in presynaptic excitability and postsynaptic response', Developmental Neurobiology. NIH Public Access, 74(1), pp. 1–15. doi: 10.1002/dneu.22120.

Lehmann FO and Dickinson MH (1997) 'The changes in power requirements and muscle efficiency during elevated force production in the fruit fly Drosophila melanogaster.', Journal of Experimental Biology, 200(7).

Lingle C. (1981) 'The Modulatory Action of Dopamine on Crustacean Foregut Neuromuscular Preparations', Journal of Experimental Biology, 94(1).

MacLennan DH (1990) 'Moleculartools to elucidate problems in excitation-contraction coupling', Biophysical Journal. Biophys J, 58(6), pp. 1355–1365. doi: 10.1016/S0006-3495(90)824820-6.

Marder E. et al. (2005) 'Invertebrate central pattern generation moves along', Current Biology. doi: 10.1016/j.cub.2005.08.022.

Marder E. and Bucher D. (2007) 'Understanding circuit dynamics using the stomatogastric nervous system oflobsters and crabs.', Annual review of physiology, 69(1), pp. 291–316. doi: 10.1146/annurev.physiol.69.031905.161516.

Marrus SB et al. (2004) 'Differential Localization of Glutamate Receptor Subunits atthe Drosophila Neuromuscular Junction', Journal of Neuroscience. Society for Neuroscience, 24(6), pp. 1406–1415. doi: 10.1523/JNEUR0SCI.1575-03.2004. [PubMed: 14960613]

Milakovic M. et al. (2014) 'Mode of action of a Drosophila FMRFamide in inducing muscle contraction', Journal of Experimental Biology, 217(10). doi: 10.1242/jeb.096941.

Nambu JR et al. (1988) 'Isolation and characterization of a drosophila neuropeptide gene', Neuron. Cell Press, 1(1), pp. 55–61. doi: 10.1016/0896-6273(88)90209-7.

Newman ZL et al. (2017) 'Input-Specific Plasticity and Homeostasis at the Drosophila Larval Neuromuscular Junction', Neuron. Cell Press, 93(6), pp. 1388–1404.e10. doi: 10.1016/j.neuron.2017.02.028.

Nusbaum MP, Blitz DM and Marder E. (2017) 'Functional consequences of neuropeptide and small-molecule co-transmission.', Nature reviews. Neuroscience, 18(7), pp. 389–403. doi: 10.1038/nrn.2017.56. [PubMed: 28592905]

Ormerod Jung and Mercier (2018) 'Modulation of neuromuscular synapses and contraction in Drosophila 3rd instar larvae', Journal of Neurogenetics. Taylor and Francis Ltd, pp. 183–194. doi: 10.1080/01677063.2018.1502761. [PubMed: 30303434]

Ormerod KG et al. (2013) 'Action of octopamine and tyramine on muscles of Drosophila melanogaster larvae', Journal of Neurophysiology, 110(8). doi: 10.1152/jn.00431.2013.

Ormerod KG et al. (2016) 'Characterizing the physiological and behavioral roles of proctolin in Drosophila melanogaster', Journal of Neurophysiology, 115(1), pp. 568–580. doi:10.1152/jn.00606.2015. [PubMed: 26538605]

Ormerod KG, Jung J. and Mercier AJ (2018) 'Modulation of neuromuscular synapses and contraction in Drosophila 3rd instar larvae', Journal of Neurogenetics. Taylor and Francis Ltd, pp. 183–194. doi: 10.1080/01677063.2018.1502761. [PubMed: 30303434]

Ormerod KG, Krans JL and Mercier AJ (2015) 'Cell-selective modulation of the Drosophila neuromuscular system by a neuropeptide', Journal of Neurophysiology, 113(5). doi:10.1152/jn.00625.2014.

Otsuka M, Kravitz E. and Potter D. (1967) 'Physiological and chemical architecture of a lobster ganglion with particular reference to gamma-aminobutyrate and glutamate', Journal of neurophysiology. J Neurophysiol, 30(4), pp. 725–752. doi: 10.1152/JN.1967.30.4.725. [PubMed: 6035690]

Paterson BA, Anikin IM and Krans JL (2010) 'Hysteresis in the production of force by larval Dipteran muscle', Journal of Experimental Biology. The Company of Biologists, 213(14), pp. 2483–943 2493. doi: 10.1242/JEB.043026.

Petzold BC et al. (2011) 'Caenorhabditis elegans Body Mechanics Are Regulated by Body Wall Muscle Tone', Biophysical Journal. The Biophysical Society, 100(8), p. 1977. doi:10.1016/J.BPJ.2011.02.035.

Picciotto MR, Higley MJ and Mineur YS (2012) 'Acetylcholine as a Neuromodulator: Cholinergic Signaling Shapes Nervous System Function and Behavior', Neuron. NIH Public Access, pp. 116–129. doi: 10.1016/j.neuron.2012.08.036.

Putney J. and Biancri C. (1974) 'Site of action of dantrolene in frog sartorius muscle', The Journal of pharmacology and experimental therapeutics. J Pharmacol Exp Ther, 189(1), pp. 202–212. Available at: https://pubmed.ncbi.nlm.nih.gov/4545054/ (Accessed: 22 September 2021). [PubMed: 4545054]

Reite OB (1972) 'Comparative physiology of histamine.', Physiological reviews, pp. 778–819. doi:10.1152/physrev.1972.52.3.778. [PubMed: 4555517]

Reuben J. et al. (1967) 'Excitation-contraction coupling in crayfish', American zoologist. Am Zool, 7(3), pp. 623–645. doi: 10.1093/ICB/7.3.623. [PubMed: 6077382]

Robbins J. (1959) 'The excitation and inhibition of crustacean muscle by amino acids', The Journal of Physiology, 148(1), pp. 39–50. doi: 10.1113/jphysiol.1959.sp006272. [PubMed: 14437751]

Roche JP et al. (2002) 'Regulation of synaptic plasticity and synaptic vesicle dynamics by the PDZ protein scribble', Journal of Neuroscience, 22(15), pp. 6471–6479. doi: 10.1523/jneurosci.22-15-06471.2002. [PubMed: 12151526]

Rohrbough J. et al. (1999) 'latheo, a Drosophila gene involved in learning, regulates functional synaptic plasticity', Neuron. Cell Press, 23(1), pp. 55–70. doi: 10.1016/S0896-6273(00)80753-9.

Saraswati S. et al. (2004) 'Tyramine and octopamine have opposite effects on the locomotion of Drosophila larvae.', Journal of neurobiology, 58(4), pp. 425–41. doi: 10.1002/neu.10298. [PubMed: 14978721]

Schwarz O. et al. (2017) 'Motor control of Drosophila feeding behavior', eLife. eLife Sciences Publications Ltd, 6. doi: 10.7554/eLife.19892.

Selverston AI (1980) 'Are central pattern generators understandable?', Behavioral and Brain Sciences, 3(4), pp. 535–540. doi: 10.1017/S0140525X00006580.

Selverston AI (2010) 'Invertebrate central pattern generator circuits.', Philosophical transactions of the Royal Society of London. Series B, Biological sciences, 365(1551), pp. 2329–45. doi:10.1098/rstb.2009.0270. [PubMed: 20603355]

Sherman R. and Atwood HL (1971) 'Synaptic facilitation: long-term neuromuscular facilitation in crustaceans', Science (New York, N.Y.). Science, 171(3977), pp. 1248–1250. doi:10.1126/SCIENCE.171.3977.1248. [PubMed: 5545202]

Singhania A. and Grueber WB (2014) 'Development of the embryonic and larval peripheral nervous system of Drosophila', Wiley Interdisciplinary Reviews: Developmental Biology. John Wiley and Sons Inc, 3(3), pp. 193–210. doi: 10.1002/wdev.135.

Smith JS et al. (1988) 'Purified ryanodine receptor from rabbit skeletal muscle is the calcium-release channel of sarcoplasmic reticulum', Journal of General Physiology. J Gen Physiol, 92(1), pp. 1–26. doi:10.1085/jgp.92.1.1.

Song W. et al. (2007) 'Peripheral multidendritic sensory neurons are necessary for rhythmic locomotion behavior in Drosophila larvae', Proceedings of the National Academy of Sciences of the United States of America, 104(12), pp. 5199–5204. doi: 10.1073/pnas.0700895104. [PubMed: 17360325]

Squire J. (2019) 'Special issue: The actin-myosin interaction in muscle: Background and overview', International Journal of Molecular Sciences. MDPI AG. doi: 10.3390/ijms20225715.

Sun X. et al. (2020) 'A neuromechanical model and kinematic analyses for Drosophila larval crawling based on physical measurements', bioRxiv. doi: 10.1101/2020.07.17.208611.

Taghert PH and Schneider LE (1990) 'Interspecific comparison of a Drosophila gene encoding FMRFamide-related neuropeptides', Journal of Neuroscience. Society for Neuroscience, 10(6), pp. 1929–1942. doi: 10.1523/jneurosci.10-06-01929.1990. [PubMed: 2113087]

Tajiri R. et al. (2017) 'Mechanical Control ofWhole Body Shape by a Single Cuticular Protein Obstructor-E in Drosophila melanogaster', PLOS Genetics. Public Library of Science, 13(1), p. e1006548. doi: 10.1371/J0URNAL.PGEN.1006548.

Taylor MV (2013) 'Comparison of Muscle Development in Drosophila and Vertebrates'. Landes Bioscience. Available at: https://www.ncbi.nlm.nih.gov/books/NBK6226/ (Accessed: 6 May 2021).

Terry RL, Kaneb HM and Wells DJ (2014) 'Poloxomer 188 Has a Deleterious Effect on Dystrophic Skeletal Muscle Function', PLoS ONE. Public Library of Science, 9(3). doi:10.1371/journal.pone.0091221.

Usherwood PNR (1967) 'Insect Neuromuscular Mechanisms', AM. Zooi.or.isT, 7, pp. 553–582. Available at: https://academic.oup.com/icb/article/7/3/553/245426 (Accessed: 20 September 2021).

Weber A. and Hertz R. (1968) 'The Relationship between Caffeine Contracture oflntact Muscle and the Effect of Caffeine on Reticulum', The Journal of general physiology, 52, pp. 750–759. [PubMed: 5688082]

Weber A, Herz R. and Reiss I. (1963) 'On the mechanism of the relaxing effect of fragmented sarcoplasmic reticulum.', The Journal of general physiology. The Rockefeller University Press, 46(4), pp. 679–702. doi: 10.1085/jgp.46.4.679. [PubMed: 13999359]

Weiss S. et al. (2019) 'Glial Ca2+signaling links endocytosis to K+buffering around neuronal somas to regulate excitability', eLife, 8. doi: 10.7554/eLife.44186.

Worden MK (1998) 'Modulation of vertebrate and invertebrate neuromuscular junctions', Current Opinion in Neurobiology. Current Biology Ltd, 8(6), pp. 740–745. doi: 10.1016/S0959-4388(98)80116-5. [PubMed: 9914241]

Zarin AA et al. (2019) 'A multilayer circuit architecture for the generation of distinct locomotor behaviors in Drosophila', eLife. eLife Sciences Publications Ltd, 8. doi: 10.7554/eLife.51781.

Zhong Y. and Peña LA (1995) 'A novel synaptic transmission mediated by a PACAP-like neuropeptide in drosophila', Neuron, 14(3), pp. 527–536. doi: 10.1016/0896-6273(95)90309-7. [PubMed: 7695899]

Key points summary

- Larval muscle contraction force increases with stimulation frequency and duration, revealing substantial plasticity between 5 and 40 Hz.
- Fictive contraction recordings demonstrate endogenous motoneuron burst frequencies consistent with the neuromuscular system operating within the range of greatest plasticity.
- Genetic and pharmacological manipulation of critical components of pre- and post-synaptic Ca^{2+} regulation significantly impact the strength and time-course of muscle contractions.
- A screen for modulators of the excitation-contraction machinery identified a FMRFa peptide, TPAEDFMRFa, and its associated signaling pathway that dramatically increases muscle performance.
- *Drosophila* serves as an excellent model for dissecting components of the excitation-contraction coupling machinery.

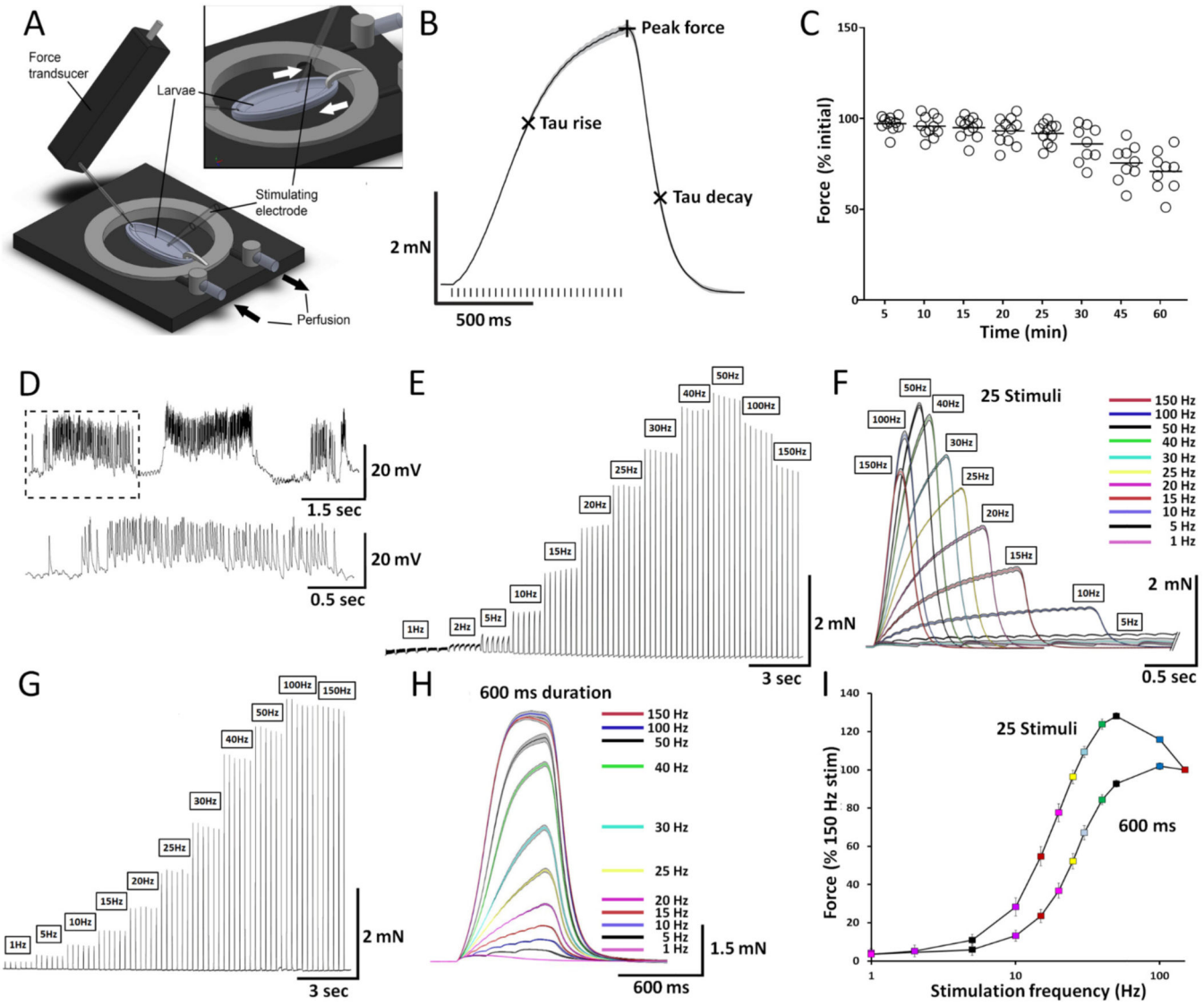

Figure 1.

Muscle contraction dynamics from 3rd instar larvae. **A)** 3D schematic of the experimental setup highlighting the force transducer, temperature-controlled holder with perfusion system, suction electrode, and 3rd instar larva. B) Representative trace from a single contraction elicited at 40 Hz for 750 ms. Contractions were generated by stimulating abdominal motoneurons in a minimum of 5 segments per experiment. Crosshairs indicate metrics derived from each contraction used for subsequent analyses. **C)** Percent of initial contraction force for steady-state recordings from control Canton S larvae elicited with 40 Hz stimulation for 600 ms every 15 s. Circles denote individual replicate recordings plotted as a percentage change in contraction amplitude compared to the initial contraction. N=9–11. **D)** Representative intracellular voltage recording from muscle fiber 6 demonstrating CPG firing patterns from a larva with the CNS left intact. The dashed box in the upper trace is expanded below. **E)** Larval motoneuron stimulation paradigm used to generate dynamic force-frequency recordings for muscle contraction from initial threshold through saturation

(1–150 Hz). Stimulus number was kept constant at 25. **F)** Six replicate contractions from each stimulation frequency in panel E were averaged and plotted with the associated 95% CI. **G)** Results using dynamic force-frequency motoneuron stimulation paradigm where stimulus duration was kept constant at 600 ms. **H)** 6 replicate contractions from each stimulation frequency in panel G were averaged and plotted with 95% CI. **I)** Muscle force versus stimulation frequency from each of the stimulation paradigms depicted in E-H is shown (25 stimuli: intraburst duration consisted of 25 stimuli at each stimulus frequency, N=10, 6 replicate contractions were elicited at each stimulation frequency and averaged for each animal. 600 ms duration: intraburst duration at each frequency was 600 ms in duration, 6 replicate contractions were elicited at each stimulation frequency and averaged for each animal, N=20).

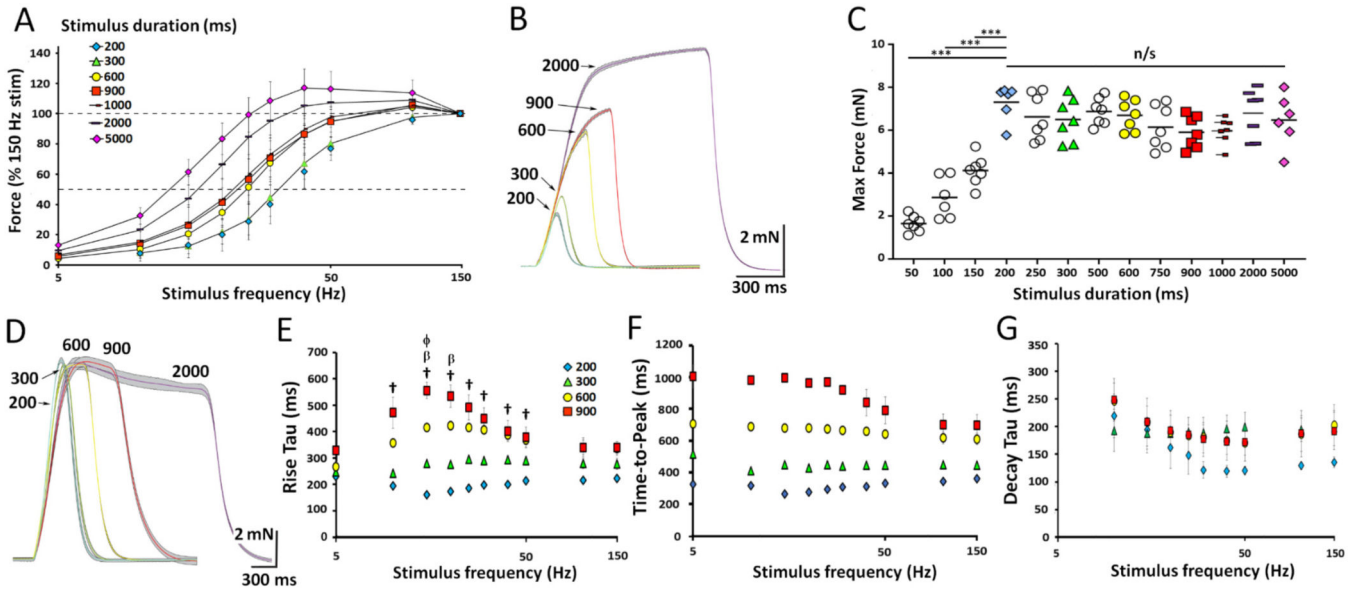

Figure 2.

Effects of stimulus duration or frequency on muscle contraction. **A)** Cumulative force-frequency plots showing the effects of varying the stimulus duration from 200 ms to 5000 ms (N=7–10). **B)** Representative traces for 25 Hz stimulation for 200, 300, 600, 900, and 2000 ms stimulus duration. **C)** Maximal force generated from a 150 Hz stimulation frequency from each replicate larva for each of the 13 different stimulation durations (one-way ANOVA, P<0.001, F=26.14, n=6–7,***P<0.0001). **D)** Representative single contraction traces from 200, 300, 600, 900, and 2000 ms duration stimuli at 150 Hz. **E)** Rise tau as function of stimulus frequency for stimulation frequencies of 200, 300, 600, and 900 ms. †, β, ϕ denote significant differences between 200 and 900, 300 and 600, and 600 and 900 respectively (One-way ANOVA, P<0.0001, F=19.12, N=3; 200 vs 900: 10 Hz P>0.0001, 15 Hz P>0.0001, 20 Hz P>0.0001, 25 Hz P>0.0001, 30 Hz P>0.0001, 40 Hz P>0.0001, 50 Hz P=0.0019; 300 vs 600 15 Hz P= 0.0416, 20 Hz P=0.0117; 600 vs 900 15Hz P=0.022). **F)** Time-to-peak as a function of stimulus frequency plots depicting data for the 200, 300, 600, and 900 ms stimulation. **G)** Decay tau versus stimulation frequency for 200, 300, 600, and 900ms stimulation groups.

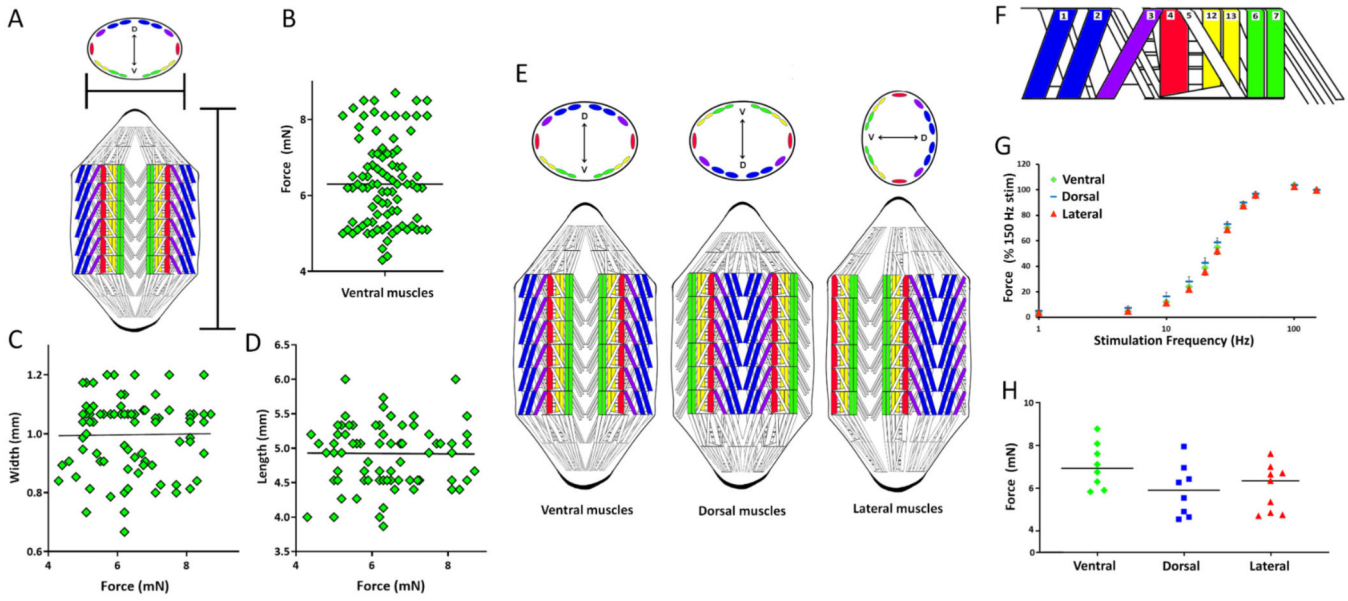

Figure 3.

Muscle force generation is independent of 3rd instar larval size and orientation. **A)** Schematic representation of a cross-section through a 3rd instar larval abdominal segment highlighting the main muscles contributing to longitudinal larval peristalsis. D-V represents the dorsal-ventral axis. Scale bar below indicates how length and width measurements were taken. **B)** Summary of maximal force values obtained from 100 animals dissected along the dorsal midline. **C-D)** Width and length measurements and the corresponding maximal force values obtained from 100 animals. Neither parameter correlates with maximal force generated (two-tailed Pearson's correlation; Width: r=0.01462, P=0.8906; length: r=−0.009, P=0.9325). **E)** Schematic representation of cross-sections through larvae from three different orientations highlighting the dominant muscles contributing to force measurements in each condition. Blue denotes muscles along the dorsal axis, green denotes muscles along the ventral axis, and red denotes muscles along the medial axis. **F)** Schematic depicting a single abdominal hemisegment highlighting muscle fiber number. **G)** Muscle force-frequency curves for each of the larval dissection orientations, indicating muscle contraction force-frequency is similar across the different fibers. **H)** Maximal force generated from a 150 Hz stimulus at 600 ms duration in each of the three different orientations shows no significant differences (One-way ANOVA, N=8, P=0.4037, F=0.915).

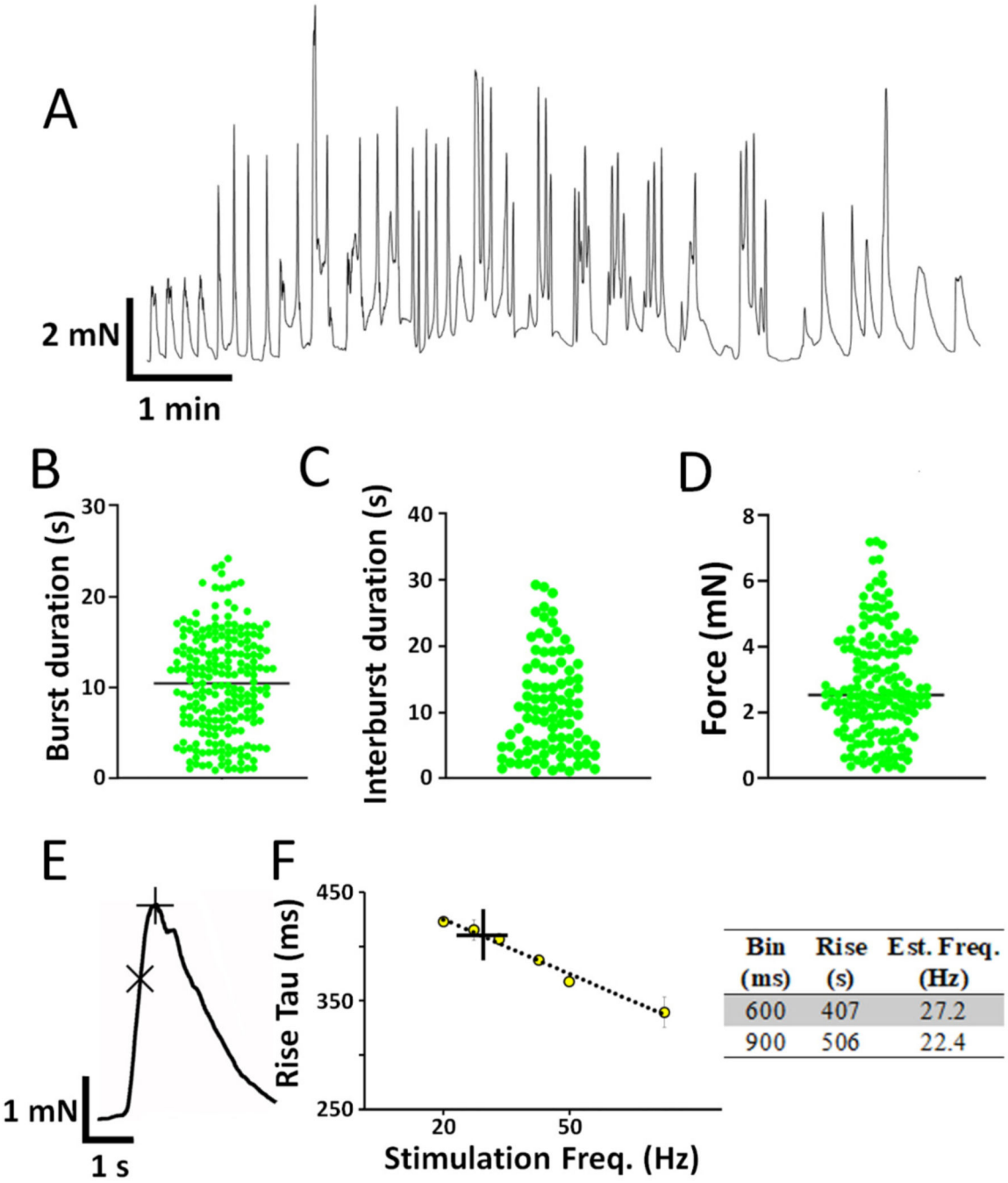

Bin (ms)	Rise (s)	Est. Freq. (Hz)
600	407	27.2
900	506	22.4

Figure 4.

Fictive recordings from larvae reveal endogenous contraction dynamics. **A)** Representative recording show the typical time-course and magnitude of fictive contractions from larvae. Individual burst durations **(B)** interburst duration vs. number of observations **(C)** and the magnitude of force contraction **(D)** was plotted from fictive contraction recordings from 3rd instar larvae (N=7). **E)** Representative single component fictive contraction profile used for kinetic calculations. **F)** Data from figure 2E replotted to show rise tau kinetics for contractions elicited from 600 ms duration stimulation for 20–100 Hz. Inset table shows the

average rise time kinetics for single component fictive contractions from data sets binned into 600 and 900 ms time-to-peak. The value for the 600 ms binned data is plotted along the trendline in **F**, as a plus symbol.

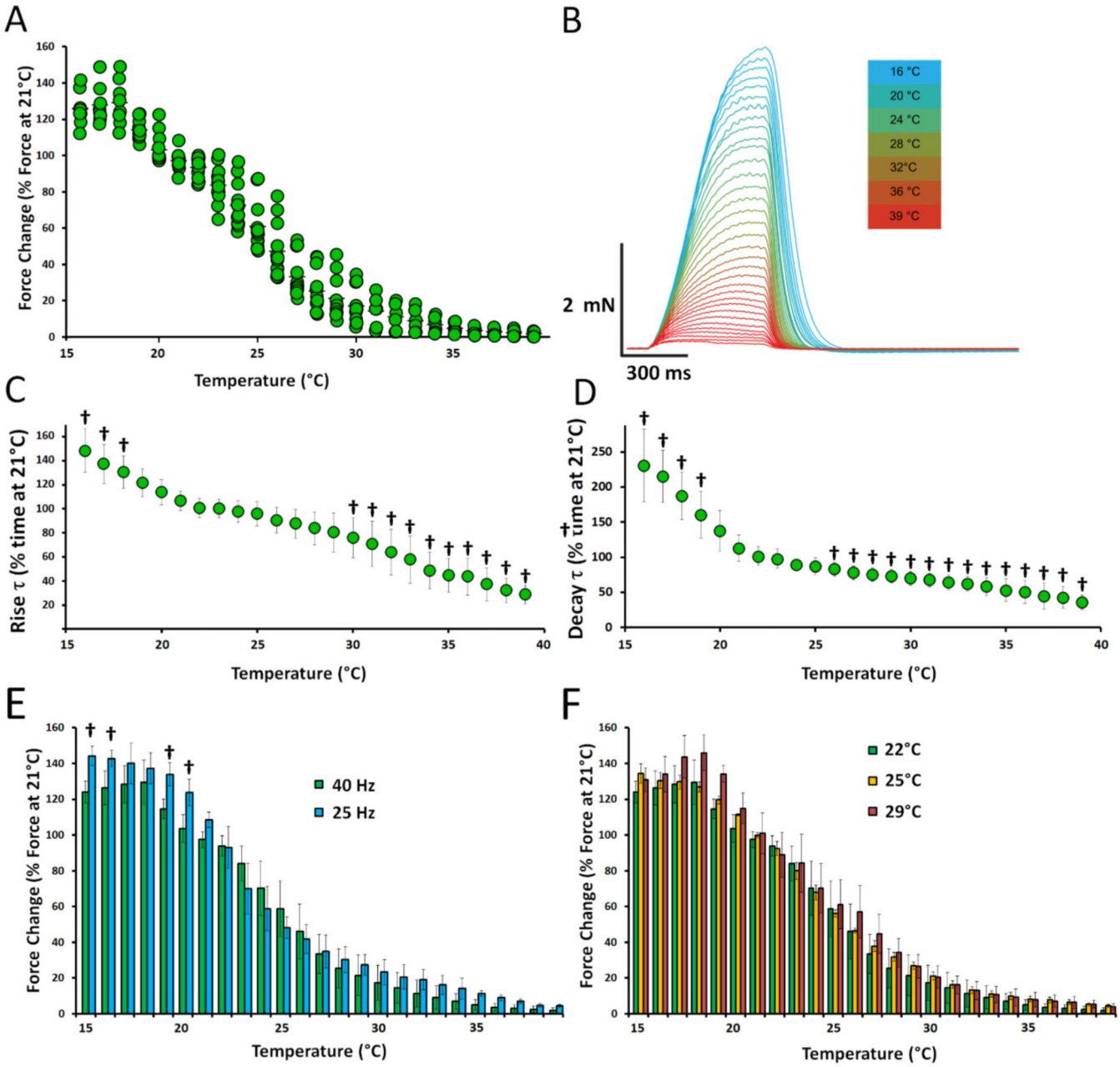

Figure 5.

Effects of temperature on muscle contraction force. **A)** Force of muscle contraction as a function of temperature. Contractions were elicited using a 40 Hz 600 ms duration stimulus given continuously throughout the experiment as temperature was varied. **B)** Color-coded individual traces from a representative experiment depicting the effects of temperature on contraction amplitude**. C-D)** Rise tau data **C)** (one-way ANOVA, P<0.0001, F=54.23; P values for 21°C vs: 16°C P>0.0001, 17°C P=0.002, 30°C P=0.0018, 31–39°C P>0.0001) and decay tau **D)** (one-way ANOVA, P<0.0001, F=32.1, P values for 21°C vs: 16–19°C P>0.0001, 26°C P=0.0016, 27°C P=0.002, 28–39°C P>0.0001) from **5A** plotted as a percentage of the time-value at 21°C, significant differences denoted with a †. **E)** Histogram

showing the effect of temperature on muscle contractions elicited using 25 Hz or 40 Hz stimulation for 600 ms duration (One-way ANOVA, $P<0.0001$, $F=205.7$; P-values: 15°C $P=0.0136$, 16°C $P=0.0354$, 19°C $P=0.0471$, 20°C $P=0.0184$), significant differences denoted with a †. **F)** Effects of thermal acclimation on muscle contraction force assayed in larvae from stocks reared for 3 generations at 22, 25, or 29°C.

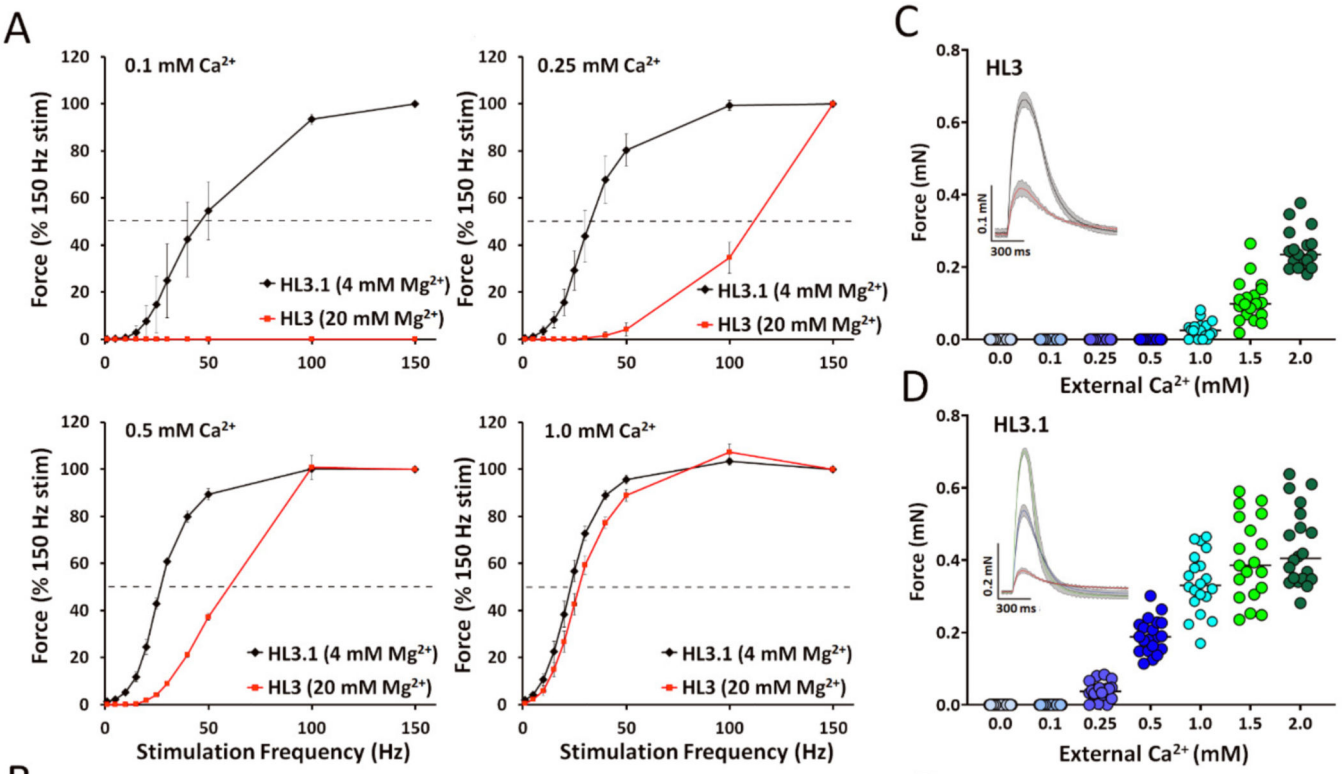

B

½ maximal stim freq		External Calcium Concentration (mM) 0.1	0.25	0.5	1	1.5	2
HL3.1	200	100.2	58.5	40	49.71	39.88	30.14
	300	100.3	53.42	49.8	40.03	30.16	31.94
	600	49.99	30.1	25.11	24.93	25	20.05
	900	50.02	30.08	24.94	20.01	24.93	20
HL3	200	n/a	100.3	99.98	50.04	49.75	39.95
	300	n/a	100.3	87.95	39.96	30.11	30.11
	600	n/a	100.3	50.28	29.89	20.34	20.2
	900	n/a	79.65	50.16	25.41	20.06	19.96

Stimulation Freq. (Hz)

Legend: 100, 80, 60, 40, 20

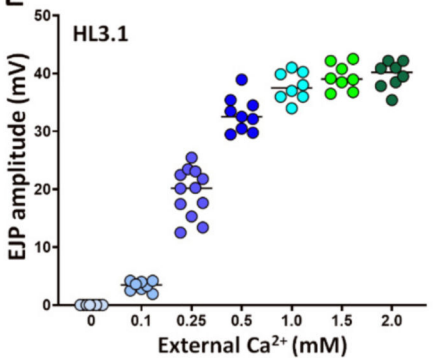

Figure 6.

Effects of external Ca^{2+} and Mg^{2+} on muscle contraction force. **A)** Force-frequency curves generated using a 600 ms duration stimulus for two physiological salines, HL3 (20 mM Mg^{2+}) and HL3.1 (4 mM Mg^{2+}) in 0.1 mM $[Ca^{2+}]_o$, 0.25 mM $[Ca^{2+}]_o$, 0.5 mM $[Ca^{2+}]_o$, and 1.0 mM $[Ca^{2+}]_o$. **B)** Half-maximal stimulation frequency required to generate 50% of the maximal force observed for each stimulus duration, $[Ca^{2+}]o$, and saline is shown. The data was obtained from force frequency curves generated using 200, 300, 600, and 900 ms stimulation duration for both physiological salines in 6 different $[Ca^{2+}]_o$. **C)** Force values generated from single motoneuron stimuli in 7 different $[Ca^{2+}]_o$ in) HL3, and. Inset: representative force traces from 1.0 and 2.0 mM $[Ca^{2+}]_o$. **D)** Force values generated from single motoneuron stimuli in 7 different $[Ca^{2+}]_o$ in HL3.1. Inset: representative force traces from 0.25, 0.5, and 2.0 mM $[Ca^{2+}]_o$. **E)** EJPs amplitude values obtained from the 7 different $[Ca^{2+}]_o$ in HL3.1.

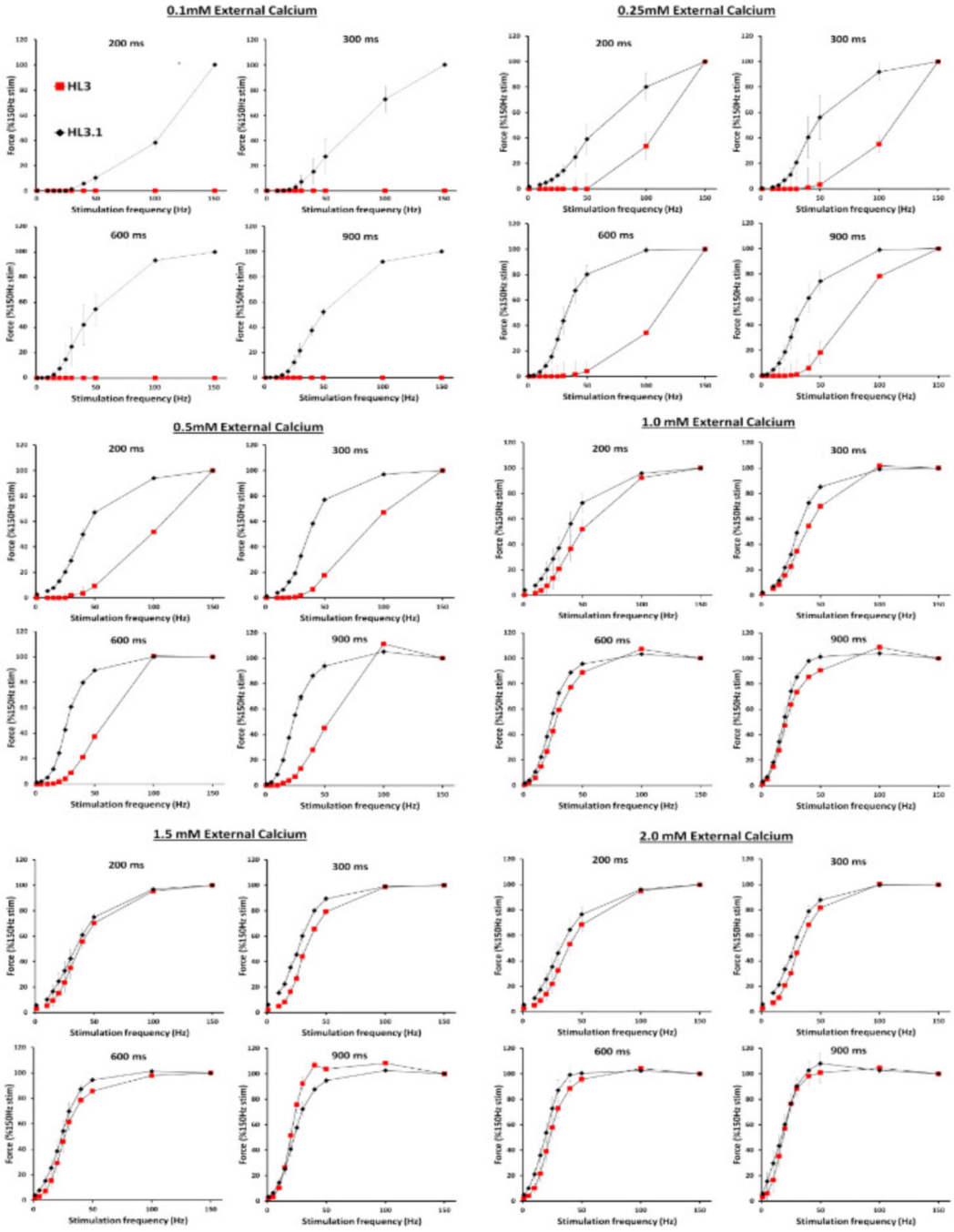

Figure 7:

Effects of external Ca^{2+} and Mg^{2+} on muscle contraction force. Force-frequency curves generated using 200, 300, 600, and 900 ms duration stimuli for two physiological salines, HL3 (20 mM Mg^{2+}) and HL3.1 (4 mM Mg^{2+}) in 0.1 mM $[Ca^{2+}]_o$, 0.25 mM $[Ca^{2+}]_o$, 0.5 mM $[Ca^{2+}]_o$, 1.0 mM $[Ca^{2+}]_o$ and 2.0 mM $[Ca^{2+}]_o$.

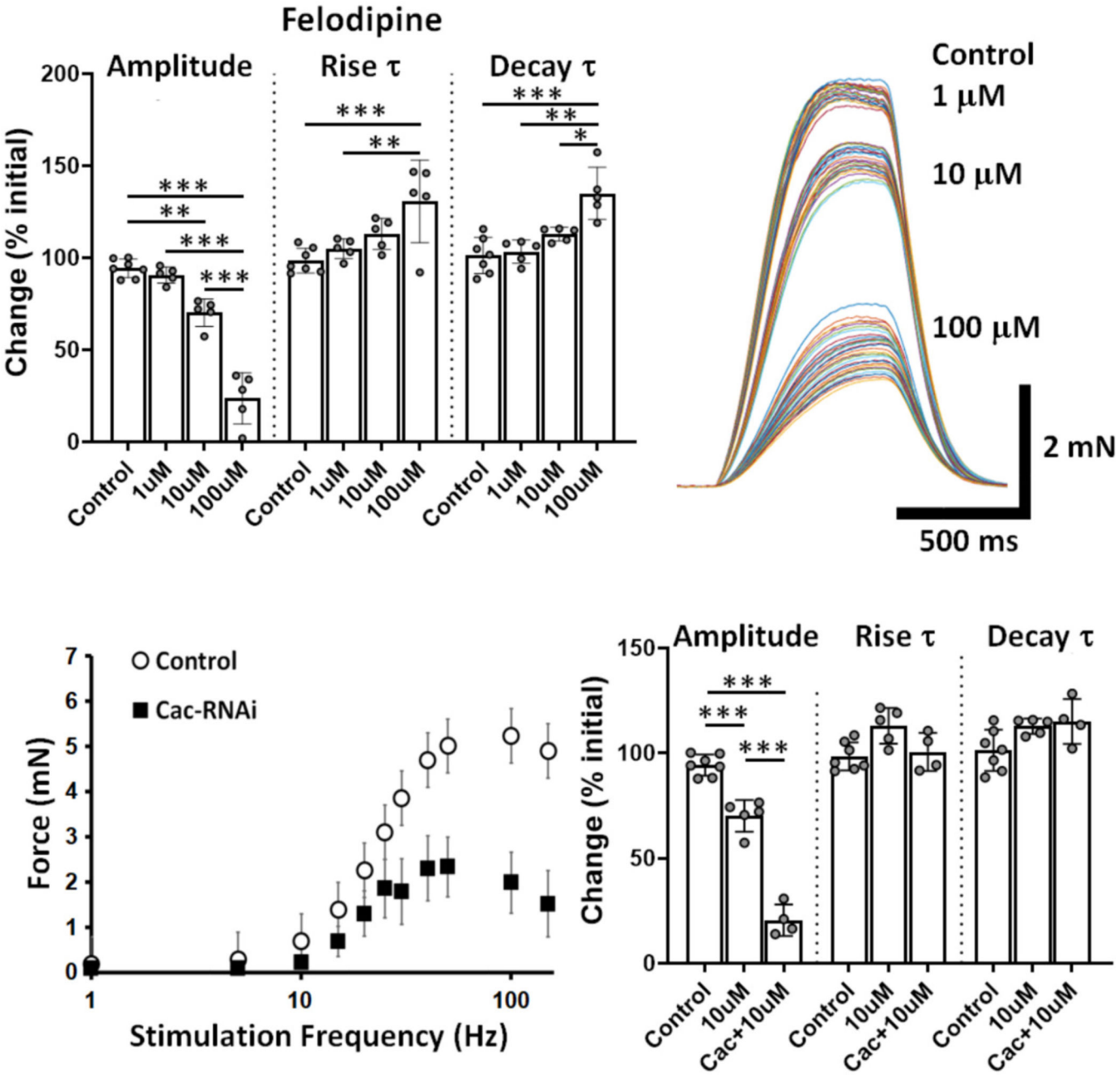

Figure 8.

The role of pre- and postsynaptic Ca^{2}+ channels on excitation-contraction coupling. **A)** Effects of 3 different concentrations of felodipine on the amplitude, rise tau, and decay tau of contractions elicited at 40 Hz for 600 ms (one-way ANOVA, P<0.0001, F=41.65, ***P>0.0001, Amplitude: C vs 10 µM P=0.0076, Rise: 1 µM vs 100 µM P=0.0087 Decay: 1 µM vs 100 µM P=0.0004, 10 µM vs 100 µM P=0.043). Inset demonstrates multiple representative contractions from control recordings in saline, and recordings in the presence of 1 µM, 10 µM, and 100µM felodipine. **B)** Force-frequency curves plotted from control Canton S and Cac-RNAi;;*elav*-Gal4 larvae. **C)** Effects of 10 µM felodipine on contractions

elicited from recordings in control and Cac-RNAi;;*elav*-Gal4 larvae (one-way ANOVA, P<0.0001, F=63.73, ***P>0.0001).

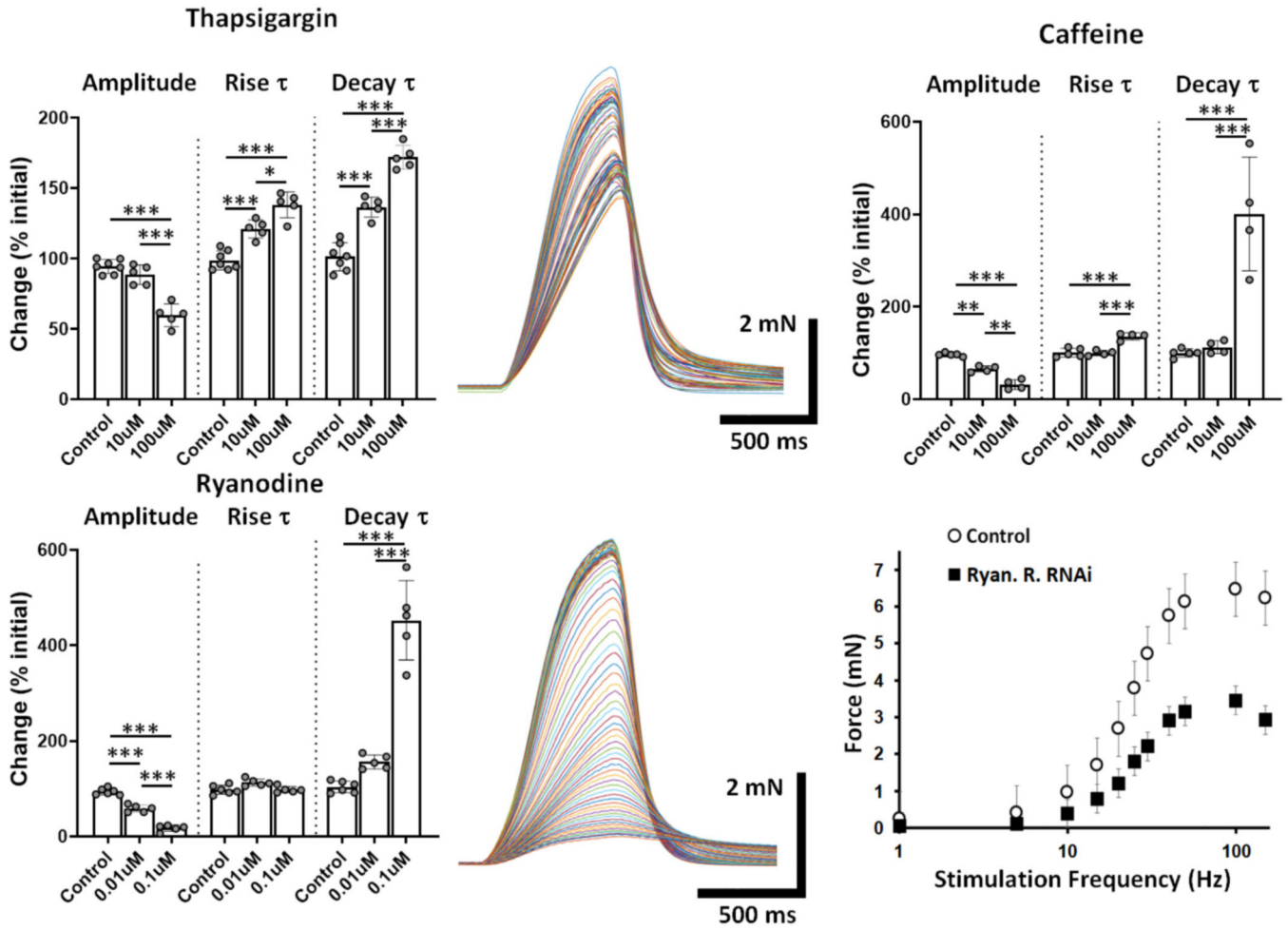

Figure 9.

The role of SR Ca^{2+} in regulating muscle contraction. **A)** Effects of 2 different concentrations of thapsigargin on the amplitude, rise tau, and decay tau of contractions at 40 Hz stimulation for 600 ms (one-way ANOVA, P<0.0001, F=96.6, ***P>0.0001, Rise 10 μM vs 100 μM P=0.0256). Inset: representative recording showing the progressive effect of 100 μM thapsigargin on contractions. **B)** Effects of 2 different concentrations of caffeine on the amplitude, rise tau, and decay tau of contractions elicited at 40 Hz stimulation for 600 ms (one-way ANOVA, P<0.0001, F=91.6; ***P<0.0001, Amplitude C vs 10 μM P=0.0003, 10 μM vs 100 μM P=0.0001). **C)** Effects of 2 different concentrations of ryanodine on the amplitude, rise tau, and decay tau of contractions elicited at 40 Hz stimulation for 600 ms (one-way ANOVA, P<0.0001, F=101.6; ***P>0.0001). Inset: representative recording showing the progressive effect of 0.1 μM ryanodine on contractions. **D)** Force-frequency curves plotted from control Canton S and *mef2*-Gal4, ryanodine-RNAi larvae.

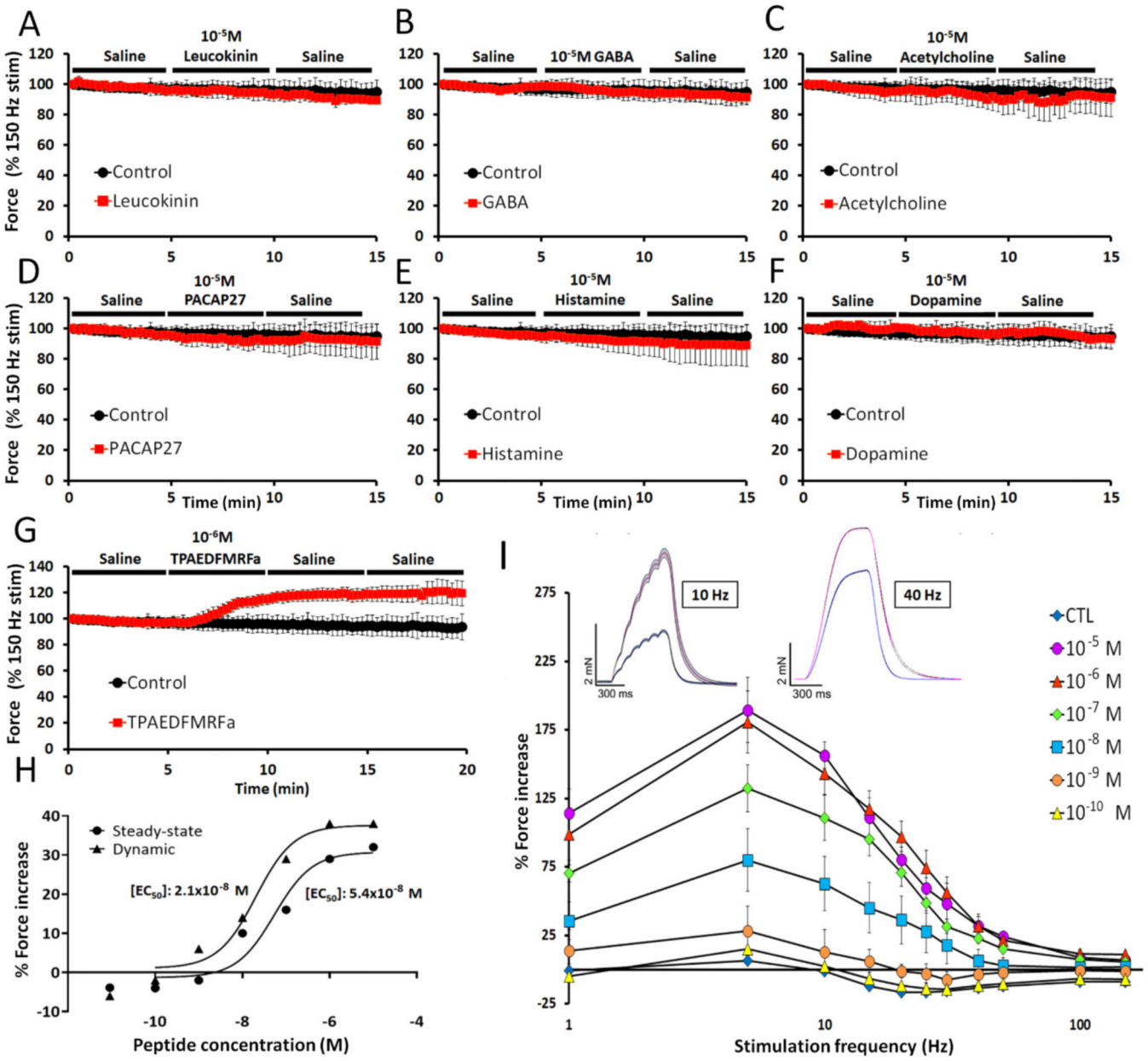

Figure 10.

Amplitude of larval contractions plotted as a function of time using a steady-state motoneuron stimulation at 40 Hz for 600 ms duration every 15s. Experiments were 15–20 minutes in duration with a constant perfusion of saline for 5 minutes followed by addition of **A)** Leucokinin, **B)** GABA, **C)** acetylcholine, **D)** PACAP27, **E)** histamine, **F)** dopamine, or **G)** TPAEDFMRFa, followed by a 5–10 min saline washout. **H)** Dose-dependent effects of TPAEDFMRFa on muscle contraction using either the steady-state or dynamic motoneuron stimulation paradigm. **I)** Dose-dependent effects of TPAEDFMRFa using the dynamic motoneuron stimulation paradigm. Inset: control (blue) vs. TPAEDFMRFa (pink) at 10 Hz and 40 Hz stimulation. One-way ANOVA, $P<0.0001$, $N=4–7$.

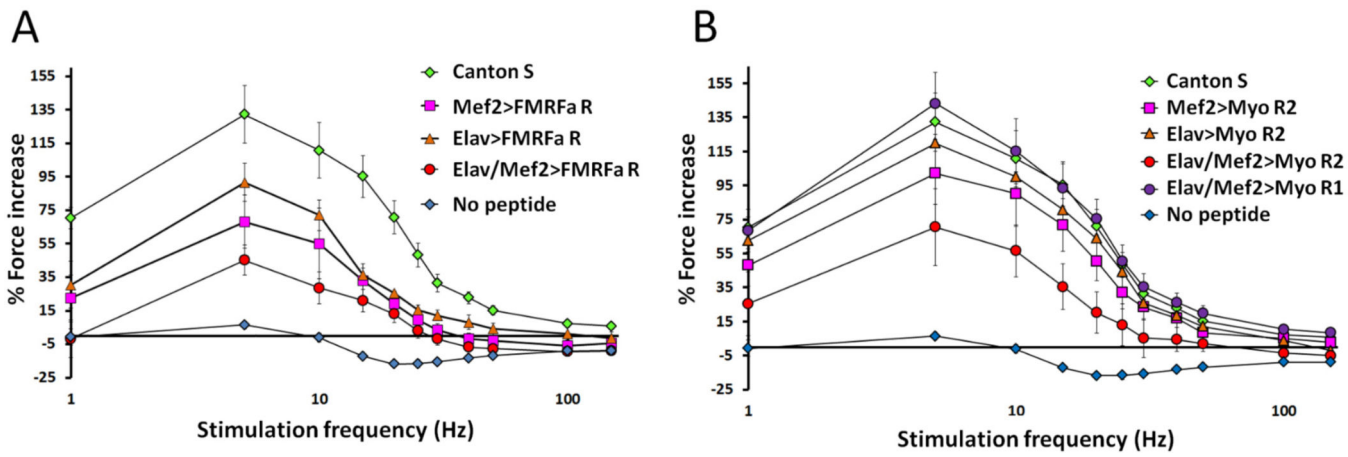

Figure 11.

Analysis of the TPAEDFMRFa pathway for enhancing contractile force at the NMJ. **A)** Force-frequency plots for the effectiveness of TPAEDFMRFa on muscle contraction force in Canton S versus larvae expressing FMRFa receptor UAS-RNAi presynaptically (Elav-GAL4), postsynaptically (Mef2-GAL4) or in both compartments. **B)** Force-frequency plots for the effectiveness of TPAEDFMRFa on muscle contraction force in Canton S versus larvae expressing Myosuppressin receptor 1 or 2 UAS-RNAi presynaptically (*elav*-Gal4), postsynaptically (*Mef2*-Gal4) or in both compartments.

Table 1:

Force-frequency values for 10 different stimulus durations calculated as a percentage of the contraction force elicited from 150 Hz stimulation. Thresholds indicate the stimulation frequency needed to elicit a visible and quantifiable contraction trace. Maximum or saturation force value indicates the frequency required to elicit a contraction that is equal in magnitude or exceeds the contraction force value obtained using 150 Hz stimulation. The EC_{50} denotes the stimulation frequency required to generate a contraction that is 50% of maximal force value obtained using 150 Hz, calculated from the force-frequency plots using GraphPad Prism.

Duration (ms) / Frequency(Hz)	200	250	300	500	600	750	900	1000	2000	5000
1	3.08 ± 2.44	3.26 ± 1.75	2.97 ± 1.30	3.03 ± 1.55	2.82 ± 1.03	2.83 ± 2.32	2.60 ± 1.29	3.48 ± 1.17†	4.57 ± 1.41*	5.93 ± 1.59*
5	-	-	-	4.56 ± 2.56	4.33 ± 1.59	5.72 ± 5.69	5.75 ± 3.90	6.79 ± 2.87	9.47 ± 3.51	13.14 ± 3.37
10	7.66 ± 5.11	6.05 ± 3.07	8.12 ± 3.62	11.28 ± 5.59	10.4 ± 3.76	13.9 ± 12.30	14.32 ± 9.20	15.33 ± 6.84	23.32 ± 9.28	32.50 ± 5.60
15	12.99 ± 8.28	10.48 ± 4.45	12.44 ±4.99	19.37 ± 7.84	20.50 ± 6.09	25.01 ± 16.35	26.04 ± 13.69	27.68 ± 10.54	43.71 ± 14.87	61.28 ± 8.40
20	20.01 ± 10.82	20.78 ± 7018	21.72 ± 7.93	32.22 ± 10.36	34.58 ± 8.40	38.65 ± 17.55	41.22 ± 16.10	43.35 ± 13.11	66.39 ± 15.50	83.40 ± 10.41
25	28.85 ± 12.31	29.80 ± 8.33	30.13 ± 10.13	46.15 ± 10.63	51.28 ± 9.51	51.71 ± 15.82	56.48 ± 16.51	59.71 ± 13.39	84.53 ± 14.45	99.13 ± 11.54
30	40.03 ± 12.88	40.33 ± 8.83	44.48 ± 12.41	62.66 ± 9.25	67.25 ± 9.20	64.89 ± 12.29	70.55 ± 15.29	73.21 ± 10.87	95.02 ± 13.04	108.43 ± 12.69
40	61.73 ± 11.10	65.57 ± 8.23	67.08 ± 10.43	81.95 ± 6.79	86.11 ± 6.15	80.73 ± 8.16	86.29 ± 12.36	89.67 ± 7.32	105.05 ± 11.63	116.91 ± 12.74
50	76.7 ± 7.70	77.67 ± 5.79	80.26 ± 7.57	90.90 ± 4.62	94.93 ± 3.88	90.58 ± 5.69	94.61 ± 9.69	97.70 ± 5.12	107.18 ± 9.61	116.29 ± 11.43
100	95.96 ± 2.87	97.23 ± 2.40	97.51 ± 1.88	100.98 ± 1.32	104.14 ± 5.65	103.81 ± 4.20	105.75 ± 3.92	105.20 ± 3.33	108.90 ± 6.18	113.67 ± 8.52
150	100 ± 0	100 ± 0	100 ± 0	100 ± 0	100 ± 0	100 ± 0	100 ± 0	100 ± 0	100 ± 0	100 ± 0
Threshold	1Hz	1Hz	1Hz	1Hz	1Hz	1Hz	1Hz	1Hz	1Hz	1Hz
Max/Saturated Force	150Hz	150Hz	150Hz	100Hz	100Hz	100Hz	100Hz	100Hz	40Hz	30Hz
EC_{50}	**35.56**	**34.28**	**33.35**	**26.68**	**25.37**	**25.38**	**23.84**	**23.07**	**17.47**	**14.75**

Legend: 0.00 | 25.0 | 50.0 | 75.0 | 100